



Norwegian University of
Science and Technology

Graphene Saturable Absorber Mirrors for 2-3 μm Lasers

Cherrie Sue Jing Lee

MSc in Physics

Submission date: June 2018

Supervisor: Irina T Sorokina, IFY

Norwegian University of Science and Technology
Department of Physics

Abstract

This thesis is devoted to the development of graphene saturable absorber mirrors for ultrafast applications in the mid-infrared. It covers from the fabrication of the graphene saturable absorber mirrors via graphene transfer process to the implementation of the saturable absorbers in different types of laser cavities and characterisations of their performances. The pump-probe technique is employed to obtain the recovery times of single- and double-layer graphene on different optical substrates. To understand the underlying physics of graphene's saturable absorption properties, measurements of its fast and slow relaxation times are important, especially in the mid-infrared range where there is a smaller choice of effective saturable absorbers for such wavelength range.

Acknowledgements

This thesis was made possible by my supervisor, Irina Sorokina and Nikolai Tolstik for providing excellent guidance and useful feedback throughout the entire process of this thesis.

I would also like to thank Dong Chul Kim for sharing his expertise on graphene transfer process and technical staffs at NTNU Nanolab for sharing their lab expertise.

Not forgetting my family and friends, especially Losshenee for her help in arranging this thesis.

The Research Council of Norway is acknowledged for the support to the Norwegian Micro- and Nano-Fabrication Facility, NorFab, project number 245963/F50.

Conference and Presentation

This section lists conference and presentation resulting from the work of this thesis.

N. Tolstik, C. S. J. Lee, E. Sorokin, and I. T. Sorokina, "8.6 MHz Extended Cavity Cr: ZnS Chirped-pulse Oscillator," in *CLEO: Science and Innovations*, 2018, p. SF1N. 2.

C.S.J. Lee, N. Tolstik, and I. T. Sorokina, "All-in-One Graphene-Based Dispersion Compensating Mirror," Poster Presentation at EPFL-MP1401 Winter School on Fiber Lasers, Lausanne, Switzerland, 12-16 Feb 2018.

Contents

Abstract	i
Acknowledgements	iii
Conference and Presentation.....	v
List of Figures.....	ix
List of Tables.....	xi
List of Abbreviations	xi
Chapter 1: Introduction.....	1
1.1 Motivation.....	1
1.2 Current State-of-the-Art Saturable Absorbers	1
1.3 Research Objectives	2
1.4 Thesis Overview.....	3
Chapter 2: Theoretical Background.....	5
2.1 Principles of Solid-State Laser	5
2.2 Principles of Mode-Locking	7
2.2.1 Active versus Passive Mode-Locking	9
2.2.2 Saturable Absorbers	9
2.2.3 Dispersion Compensation.....	13
2.3 Graphene as a Saturable Absorber.....	14
2.3.1 Properties of Graphene	14
2.3.2 Fabrication and Characterisation of Graphene	15
Chapter 3: Fabrication and Characterisation Methods for Graphene Saturable Absorber Mirrors	19
3.1 Graphene Transfer.....	19
3.2 Raman Spectroscopy.....	24
3.3 Discussion.....	28
Chapter 4: Experimental Setup	31
4.1 Pump-Probe Experiment.....	31
4.2 Mode-Locking in Cr:ZnS Laser.....	35
4.2.1 Standard Cr:ZnS Cavity.....	35
4.2.2 Extended Cr:ZnS Cavity	35
Chapter 5: Experimental Results and Discussion	37
5.1 Relaxation Times	37

5.1.1	SESAM and CNT.....	37
5.1.2	Graphene on Sapphire Mirrors	39
5.1.3	Graphene on Chirped Mirrors	40
5.1.4	Graphene on Silver Mirror	41
5.1.5	Summary	41
5.2	Mode-Locking in Cr:ZnS Laser.....	42
5.2.1	Graphene on Chirped Mirror.....	42
Chapter 6: Conclusion and Future Outlook		45
References.....		47
Appendix		53

List of Figures

Figure 1 Main components of a typical laser system.....	5
Figure 2. Two-, three- and four- level laser schemes.	6
Figure 3. Signals of a mode-locked laser in frequency and time domain. (a) The mode amplitudes have a Gaussian distribution with gain bandwidth, $\Delta\nu$. (b) Zero phase difference between each mode. (c) Sharp intense peak called mode-locked pulse with full width half maximum (fwhm), tp	7
Figure 4. Two possible scenarios when light passes through the saturable absorber. When the intensity of the incident light is low, the light experiences a high loss whereas when the intensity of the light is high, the light experiences a much lower loss. Figure is regenerated from [23].	10
Figure 5. The three fundamental types of mode-locking: (a) slow saturable absorber mode-locking with dynamic gain saturation, (b) fast saturable absorber mode-locking, (c) mode-locking with slow saturable absorber without dynamic gain. Image regenerated from [24].	11
Figure 6. A typical Raman spectrum of monolayer graphene with D, G and G' band located at approximately 1350 cm^{-1} , 1582 cm^{-1} and 2700 cm^{-1} respectively.	16
Figure 7. An overview of PMMA-mediated transfer of graphene. The substrate used is Si wafer.	23
Figure 8. Raman spectrum of the as-bought CVD graphene (top-side) with G and G' peaks at 1590 cm^{-1} and 2698 cm^{-1} respectively. The D band is not present.	24
Figure 9. (a) Raman spectrum and (b) optical microscope image of single-layer graphene on Ag mirror (GAM).	25
Figure 10. Raman spectra of (a) single-layer graphene on sapphire mirror 1 (GSM1) and (b) two-layer graphene on sapphire mirror 2 (GSM2).	26
Figure 11. Raman spectra of single- and two-layer graphene on chirped mirror 1 (GCM1).	27
Figure 12. Raman spectra of single- and two-layer graphene on chirped mirror 2 (GCM2).	28
Figure 13. Raman microscope image of two-layer graphene on GSM2. The graphene is folded and not continuous with cracks on the left region of the image.	29
Figure 14. The pump-probe setup. The pump beam is coloured in red while the probe beam is coloured in black.	31
Figure 15. The autocorrelator measurement of the femtosecond mode-locked pulse source with FWHM (assuming sech shape) of 63.4 fs	33
Figure 16. The autocorrelator measurement of the picosecond mode-locked pulse source with FWHM (assuming Gauss shape) of 1.6 ps	33
Figure 17. The spectrum of the mode-locked laser source.	34
Figure 18. The standard Cr:ZnS cavity for mode-locking.	35
Figure 19. The extended Cr:ZnS cavity for mode-locking.	36
Figure 20. The relaxation dynamics of SESAM at above $2\text{ }\mu\text{m}$	38
Figure 21. The relaxation dynamic of CNT at above $2\text{ }\mu\text{m}$	38
Figure 22. The relaxation dynamic of two-layer graphene on sapphire mirror 2 (GS2) at above $2\text{ }\mu\text{m}$	39
Figure 23. The relaxation dynamic of two-layer graphene on GCM1 at above $2\text{ }\mu\text{m}$	40
Figure 24. The relaxation dynamics of one- and two-layer graphene on chirped mirror 2 (GCM2) at above $2\text{ }\mu\text{m}$	40
Figure 25. The relaxation dynamics of single-layer graphene on Ag mirror (GAM) at above $2\text{ }\mu\text{m}$	41
Figure 26. Autocorrelator measurement of the pulse duration using GCM1 as saturable absorber. ...	43
Figure 27. The optical spectra of the mode-locked laser using GCM1 as saturable absorber in the standard and extended cavities.	43
Figure 28. The pulse train in the extended cavity regime.	44
Figure 29. The Raman spectrum of as-bought graphene (back-side) with D, G and G' bands at 1336 cm^{-1} , 1580 cm^{-1} and 2670 cm^{-1} respectively. $I_D/I_G = 0.676$ and $I_G/I_G' = 0.715$	53

List of Tables

Table 1. The measured and reported recovery times of SESAM and CNT.....	37
Table 2. A summary of the fast and slow components of graphene's recovery time, measured using pump-probe technique at 2.35 μm	41
Table 3. The summary of attempts to transfer graphene onto Si wafer, by changing different kind of parameters.	59

List of Abbreviations

SESAM	Semiconductor saturable absorber mirror
CNT	Carbon nanotube
APM	Additive pulse mode-locking
KLM	Kerr-lens mode-locking
GDD	Group delay dispersion
2D	Two dimensional
CVD	Chemical vapour deposition
PMMA	Polymethyl metacrylate
APS	Ammonium persulfate
GAM	Graphene on silver mirror
GS1	Graphene on sapphire mirror 1
GS2	Graphene on sapphire mirror 2
GCM1	Graphene on chirped mirror 1
GCM2	Graphene on chirped mirror 2
FWHM	Full width half maximum
YAG	Yttrium aluminium garnet

Chapter 1: Introduction

1.1 Motivation

The mid-infrared which spans from 2-20 μm is interesting because many molecules have absorption lines at this window, which is very useful for spectroscopic applications. In addition, water has strong absorption near 2 μm allows lasers at such wavelength to be used in non-invasive diagnostics in biological tissues for medical applications. In metrology, lasers above 2 μm can be used to predict weather and climate based on water vapour concentration in the atmosphere. The Earth's atmosphere which has a transparent window in the mid-infrared, requires lasers operating in such range for environmental sensing [1]. Thus, there are many strong incentives to develop lasers in the mid-infrared.

Mode-locking is a technique to generate pulse laser. A passive element known as saturable absorber is required to generate mode-locked pulses. Graphene, due to its zero bandgap can absorb at any wavelength, making it an excellent choice of saturable absorber. Graphene can be transferred onto different types of substrate mirrors such as silver mirror, sapphire mirror and even dispersion compensating mirror, known as chirped mirror. This thesis explores the possibility of such graphene-based saturable absorbers by characterising their performances as saturable absorbers for wavelength above 2 μm .

1.2 Current State-of-the-Art Saturable Absorbers

Current commercial pulse lasers are generally mode-locked by semiconductor saturable absorbers (SESAM). SESAM allows good control of saturable absorption parameters but its complex fabrication, bulky structure and narrow operating wavelength range spurred the development of other types of saturable absorbers.

Attracted to its simpler and cheaper fabrication, carbon nanotubes (CNTs) are widely used as saturable absorber especially within the fibre laser community as it is much easier to integrate CNT into the laser cavity than a SESAM.

However, compared to CNT, graphene has many more attractive features. SESAM and CNT have limited operation beyond 2 μm , whereas graphene has a wideband operation extending from the ultraviolet to far-infrared region and hence, a good choice for mode-locking in the mid-infrared.

Graphene is usually transferred onto an optical substrate such as mirror to be used as saturable absorber. Thus, the operating bandwidth of graphene is often limited by the bandwidth of the optical substrate. Mode-locking using graphene on highly reflective

mirrors at 2 μm has been demonstrated [2-4]. Graphene on special type of mirrors such as gold mirror that could support mode-locking at 2.4 μm has also been reported [5].

Besides saturable absorber, the dispersion in a laser cavity plays an important role in mode-locking. One method to compensate dispersion in a cavity is the use of dispersive dielectric mirrors or otherwise known as chirped mirrors.

Mode-locking using a chirped mirror as a dispersion compensator and a graphene saturable absorber has been demonstrated [6]. But so far, a graphene-based chirped mirror has yet to be reported. By transferring graphene which act as a saturable absorber onto a chirped mirror, a graphene-based chirped mirror is created. This multi-functional optical device could potentially open up many new possibilities leading to the realisation of compact ultrafast laser.

1.3 Research Objectives

The aim of this work is to develop cutting-edge laser technology for ultrafast application in the mid-infrared range. Thus far, graphene is the most promising candidate as a saturable absorber for passive mode-locking due to its fast recovery time. Although there is an abundant literature on graphene saturable absorber, very few are focused on mid-infrared applications, particularly the recovery times of graphene on different types of mirrors, pumped-and-probed at wavelength above 2 μm . By studying the recovery times of graphene, we hope to gain a better understanding on the physics of graphene unique saturable absorption properties.

The objectives of this work are:

1. Obtain relevant knowledge about laser physics and material physics through literature research.
2. Develop efficient fabrication of graphene saturable absorber mirrors by optimising various parameters in graphene transfer process.
3. Characterise the graphene saturable absorber mirrors using Raman spectroscopy to analyse the quality of the transferred graphene.
4. Measurement of the recovery times of the graphene saturable absorber mirrors using pump-probe technique.
5. Explore the possibility to combine the function of graphene as a saturable absorber and the function of a chirped mirror as a dispersion compensator to create an all-in-one multi-functional optical device.
6. Assess the mode-locking ability of the saturable absorbers in different types of laser cavities.

1.4 Thesis Overview

This thesis aims to provide a comprehensive understanding on graphene saturable absorber mirrors from their fabrication to their implementation in mode-locked lasers.

This thesis begins with Chapter 1, which gives an overview of the thesis and followed by Chapter 2 to introduce the main concepts on pulse lasers especially in the mid-infrared region and the role of saturable absorbers in passive mode-locking. Properties that made graphene to stand out as a saturable absorber will also be discussed.

Chapter 3 emphasises on the work that was conducted in the clean room facility to fabricate and characterise the graphene saturable absorber mirrors. The characterisation using Raman spectroscopy is discussed in this chapter whereas characterisation of the recovery times of the saturable absorber is elaborated in the next chapter.

Chapter 4 describes the experimental setup of the pump-probe technique to measure the recovery times of the graphene saturable absorber mirrors and the different types of laser cavities for mode-locking using the graphene saturable absorber mirrors.

The recovery times of the graphene saturable absorber mirrors and performance of the mode-locked lasers will be presented and compared with other available saturable absorbers in Chapter 5.

The final chapter, Chapter 6 provides a brief summary of this thesis and suggestions of some possible future work.

Chapter 2: Theoretical Background

2.1 Principles of Solid-State Laser

“Laser” is an acronym for “Light Amplification by Stimulated Emission”. Stimulated emission has the same direction, polarisation, phase and spectral characteristics as the stimulating radiation field, which contribute to the high degree of coherence of laser emission compared to any other light sources.

A typical laser consists of a gain or amplifying medium and a resonant cavity, as illustrated in Figure 1.

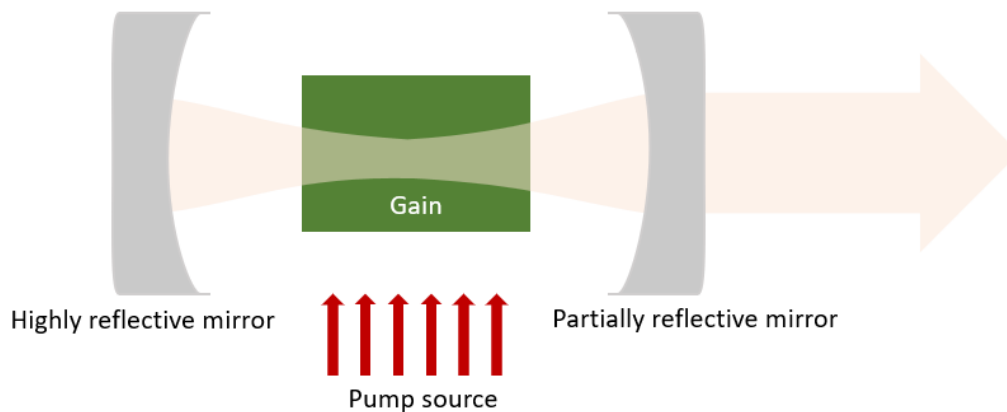


Figure 1 Main components of a typical laser system.

The intensity of light is amplified each time it passes through the gain medium. The role of the cavity is to maintain these multiple trips of light through the gain medium. To satisfy lasing condition, the gain must exceed the cavity loss and the phase shift must be an integer times 2π , after each round trip under steady-state condition.

Depending on the type of gain medium used, the laser is a solid-state laser when the gain medium is solid such as $Cr:Al_2O_3$ (ruby), $Cr:ZnS$ and many other crystals. Pumping is usually supplied by a diode laser, gas discharge lamp, or another laser at shorter wavelength to provide the energy required to transfer electrons from a lower energy level to a higher one in the gain medium, creating a so-called population inversion, whereby the number of atoms in the higher energy level, N_2 is larger than the number of atoms in the lower energy level, N_1 ($N_2 > N_1$). This is not possible in a 2-level system since excited atoms return immediately to the lower energy state, hence it is always $N_2 \leq N_1$ in a 2-level system. Population inversion is only achieved in 3-,4- or more-level systems. From Figure 2, in 3-and 4-level schemes, the number of atoms at the upper level of the laser transition is always larger than the number of atoms in the lower level of the laser transition, provided that the lifetime (τ) of the upper level is large in comparison to the relaxation time of the fast decay. The laser emission

wavelength is determined by the laser transition from the upper state to the lower state (Figure 2) [7, 8]. Different media will emit different wavelengths, for example, ruby laser has emission near 700 nm [9] and *Cr:ZnS* has emission near 2.35 μm .

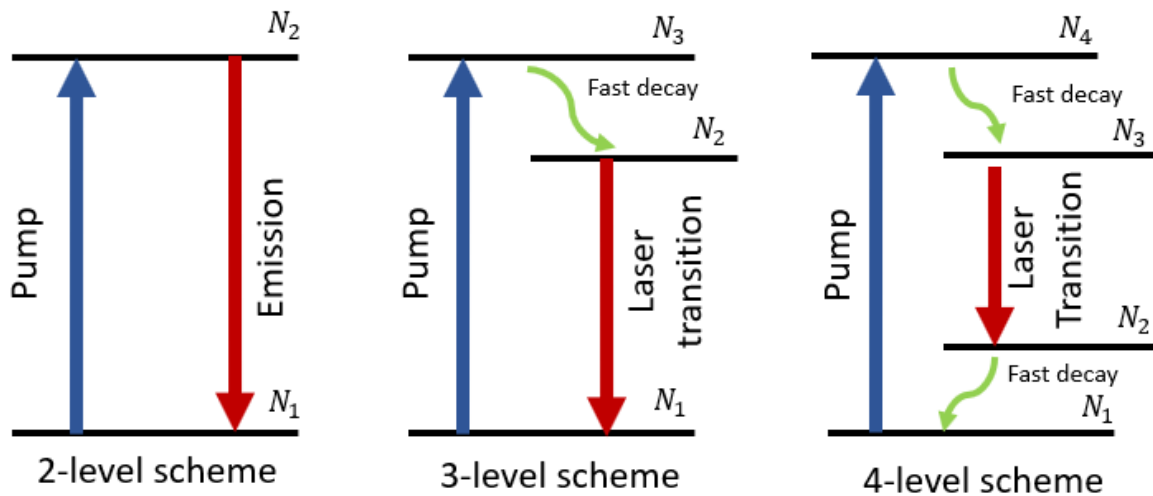


Figure 2. Two-, three- and four- level laser schemes.

The main disadvantage of the 3-level system is that laser transition occurs between the higher energy state and the ground state, requiring high pump threshold to create population inversion. This drawback is avoided in a 4-level system since the laser transition does not involve the ground state directly. Nevertheless, the first ever laser demonstrated is the ruby laser, a 3-level laser. For high peak power applications, 3-level system is a better choice since it experiences lesser non-radiative loss. However, for the purpose of this work, the pump threshold, emission wavelength and the large bandwidth provided by vibronic crystals are more critical than the output power hence, *Cr:ZnS*, a 4-level laser with emission peak at around 2.35 μm [10] was used.

***Cr:ZnS* as Gain Medium**

Before the invention of transition metal-doped zinc chalcogenides, there are not many broadband lasers in the mid-infrared range operating at room temperature. Majority of vibronic materials exhibit quenching in the mid-infrared at room temperature. Moreover, conventional semiconductor lasers at this wavelength would require cryogenic cooling and not as broadband as vibronic materials. The use of Cr^{2+} -doped chalcogenides crystals opened the possibility of having a broadband tunable laser emitting at wavelengths above 2 μm that is diode-pumpable and operating at room temperature. Furthermore, they have exceptionally broad emission bands which implies that ultrashort pulse generation such as mode-locking is possible. *Cr:ZnS* and *Cr:ZnSe* particularly stand out from this group of material due to their remarkably high fluorescence quantum yield at 300 K, has high gain cross-section and does not suffer from parasitic laser processes such as excited state absorption or upconversion [10]. The latter is a crucial factor because many promising broadband materials suffer from this upper state transition and thus reduce the number of available good laser material.

Although both *Cr:ZnS* and *Cr:ZnSe* share similar spectroscopic properties, *Cr:ZnS* has a lower thermal lensing parameter (dn/dT , where n is the refractive index and T is the temperature) of $46 \cdot 10^{-6}$ 1/K compared to $70 \cdot 10^{-6}$ 1/K in *Cr:ZnSe* [10]. Combined with its higher thermal conductivity (27 W/mK) and higher shock parameter (7.1 W/m^{1/2}), *Cr:ZnS* has better power handling capability and hence, attractive for high power applications [11-13].

2.2 Principles of Mode-Locking

Typical mechanisms to generate laser pulses are Q-switching and mode-locking. The former generates pulses in the range of nanoseconds whereas smaller pulses down to femtoseconds are possible in the latter case. For ultrafast application such as pump-probe spectroscopy, which is a part of this work, a femtosecond mode-locked laser is required.

Light oscillating between the mirrors in a laser forms longitudinal waves and in principle, can support a multiple number of modes within the gain medium's bandwidth. If these modes oscillate independently with random phase relationship, the output is a random sequence of light pulses. However, when these modes are synchronized to oscillate in a fixed phase manner, such that these modes interfere constructively and periodically, a train of well-defined pulses is produced. The laser is said to be mode-locked when this is achieved [14].

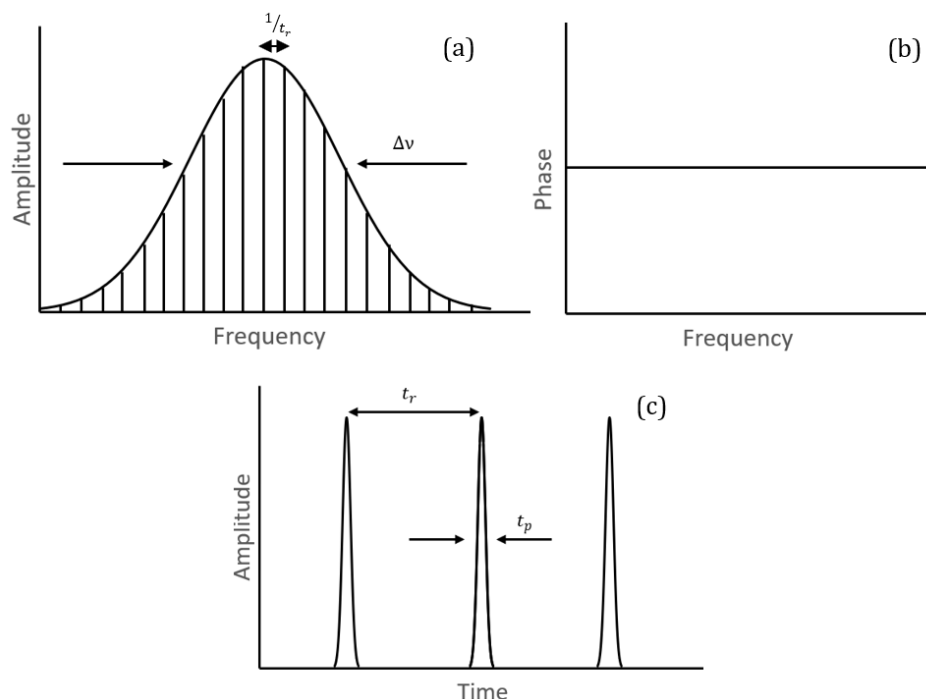


Figure 3. Signals of a mode-locked laser in frequency and time domain. (a) The mode amplitudes have a Gaussian distribution with gain bandwidth, $\Delta\nu$. (b) Zero phase difference between each mode. (c) Sharp intense peak called mode-locked pulse with full width half maximum (fwhm), t_p .

The pulse repeats itself for every cavity round-trip time. Since the pulses propagate back and forth between the two mirrors separated at length L , the repetition rate $\left(\frac{1}{t_r}\right)$ of these pulses can be written as:

$$\frac{1}{t_r} = \frac{c}{2L} \quad (1)$$

where t_r is the cavity round-trip time. From equation (1), the cavity length influences the repetition rate, and consequently influences the pulse energy (E_p) of the laser since the pulse energy is dependent on the repetition rate by this relation:

$$E_p = \frac{P_{av}}{1/t_r} \quad (2)$$

where P_{av} is the average power. The pulse energy is the energy of an optical pulse and can also be defined as the integral of peak power P_p over time.

$$P_p = \frac{E_p}{t_p} \quad (3)$$

where t_p is the full width half maximum (shown in Figure 3) and is approximately related to the gain bandwidth $\Delta\nu$, t_r and number of modes N as follow:

$$t_p \approx \frac{t_r}{N} \approx \frac{1}{\Delta\nu} \quad (4)$$

The transform limit is reached when the smallest pulse is obtained for a fixed bandwidth. $t_p \Delta\nu$ is also known as the time bandwidth product. This product is typically used to confirm a mode-locked pulse. Equation (4) also shows that to obtain narrower pulse width, larger bandwidth is required. Hence, vibronic materials which exhibit broadband emission are often used to generate mode-locked pulses with narrow pulse width. Equation (4) is a rough approximation, thus, for a Gaussian pulse, equation (4) would be [15]:

$$t_p = \frac{0.44}{\Delta\nu} \quad (5)$$

Occasionally, when the pulse is approaching the transform limit or in other word, less chirped, for instance in the case of a soliton mode-locked laser, a hyperbolic-secant is a better representation of the pulse shape and equation (4) is modified to [15]:

$$t_p = \frac{0.315}{\Delta\nu} \quad (6)$$

The difference in pulse shape affects the calculation of peak power as well. If the pulse shape is known, a numerical factor f_p is introduced into equation (3) as such:

$$P_p = f_p \frac{E_p}{t_p} \quad (7)$$

For a Gaussian-shaped pulse, $f_p = 0.94$ and $f_p = 0.88$ for hyperbolic secant pulse [16].

2.2.1 Active versus Passive Mode-Locking

To achieve mode-locking, a modulation mechanism is required to control the relative phases of the mode spectrum such that a fixed-phase relationship among the modes is established. This can be achieved by active or passive means.

In active mode-locking, the modulation is induced by an external mechanical mechanism such as acousto-optic or electro-optic modulator. The modulator controls the intracavity loss periodically such that the modulation frequency matches the cavity round-trip time. The first successful mode-locked laser was demonstrated via active mode-locking using an internal acoustic loss modulator [17]. On top of that, the first demonstration of mode-locking in *Cr:ZnSe* laser with pulse width of 4.4 ps operating near 2.5 μm was realised by active means, using an acousto-optic modulator [18]. Actively mode-locked lasers offer high degree of stability and reproducibility. However, the typical output pulses of such system have pulse widths limited to the order of picosecond. Narrower pulse widths would be challenging because as the pulse gets narrower, the pulse-shortening effect of the modulator is offset by other pulse-broadening effects such as chromatic dispersion.

On the other hand, in passive mode-locking the modulation is induced internally using *saturable absorbers*, without the need of any additional electronics. Saturable absorber varies the resonator loss depending on the intensity of light passing through it. More intensive light is able to saturate the saturable absorber which temporarily reduces the loss whereas weaker light is unable to saturate the saturable absorber and hence, experiences a greater loss. Finally, this will lead to suppression of low intensity light and intensification of high intensity peak radiation in the cavity. Due to the rapid recovery time of saturable absorber, the modulation of loss happens very fast. Combined with the fact that it is not limited by the speed of electronics like in active mode-locking, shorter pulse widths down to sub-5 fs [19, 20] is possible using passive mode-locking. Passive mode-locking in *Cr:ZnS* laser above 2 μm with pulse widths of 69 fs [21] using Kerr-lens technique and 130 fs using SESAM [22] have also been reported. Moreover, the simplistic design of passive mode-locking enables production of smaller, more compact and low-cost pulse laser system.

2.2.2 Saturable Absorbers

The intensity-dependence absorption of a saturable absorber can be described using electron density of state occupying the energy levels of the valence band E_v and the conduction band E_c of the saturable absorber. When the saturable absorber is inserted into the cavity, light with fluctuating intensities will pass through the saturable absorber.

If the intensity of the incident light is low, majority of the photons will be absorbed to excite the electrons from the valence band to the conduction band, since the electron density of states in the conduction band is less occupied. The incident photons will experience very high loss. On the other hand, in the case of high intensity of light, less photons will be absorbed because the electron density of states in the conduction band is occupied by excited electrons. The electrons are excited at a rate much higher than the rate of recombination to the valence band. Hence, the absorption is said to be saturated. At this point, incident photons will not be absorbed and experience a reduced loss. The saturable absorption mechanism is illustrated in Figure 4.

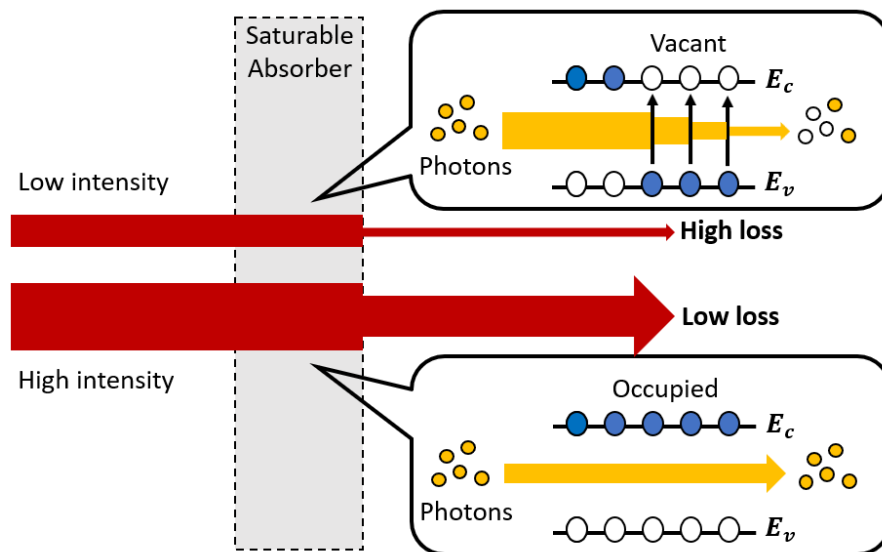


Figure 4. Two possible scenarios when light passes through the saturable absorber. When the intensity of the incident light is low, the light experiences a high loss whereas when the intensity of the light is high, the light experiences a much lower loss. Figure is regenerated from [23].

The high loss experienced by light of low intensity and low loss experienced by light of high intensity enable lower intensity components of the pulse such as continuous wave background radiation, pulse wings and pedestals to be suppressed out, whereas the high intensity fluctuations are enhanced. Consequently, after a few cavity round trips, the light fluctuations begin to oscillate as pulses.

2.2.2.1 Recovery time

The recovery time of the saturable absorber is the time taken for the saturable absorber to return from its excited state to its initial state, via various possible relaxation processes. Depending on the pulse duration of the laser, a saturable absorber is considered a *fast saturable absorber* when the recovery time is shorter than the pulse duration whereas a *slow saturable absorber* is one with recovery time longer than the pulse duration. The recovery time of a saturable absorber is an important parameter that influences the operation regime of passive mode-locking. There are 3 fundamental types of passive mode-locking namely: fast saturable absorber mode-locking, slow saturable absorber mode-locking and soliton mode-

locking. The evolution of the gain and loss in time of these 3 types are illustrated in Figure 5.

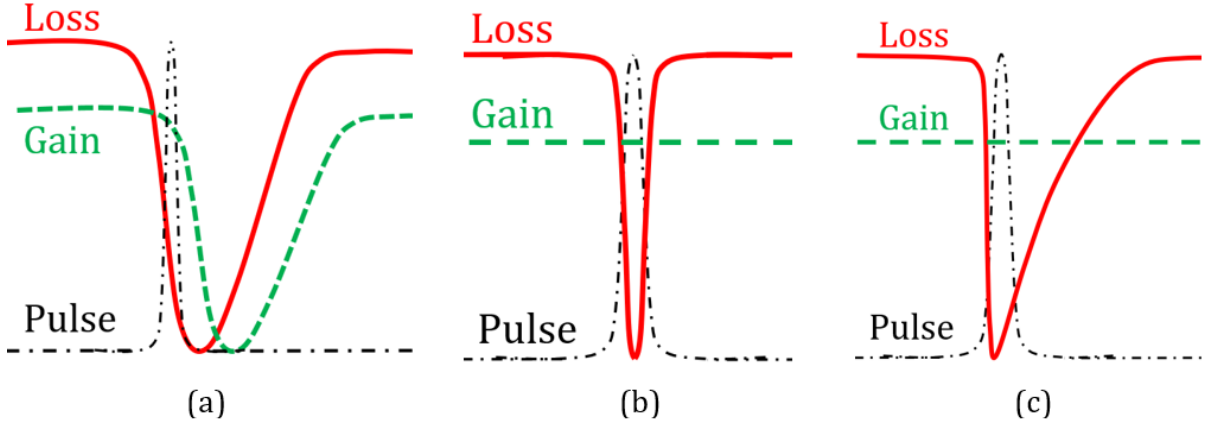


Figure 5. The three fundamental types of mode-locking: (a) slow saturable absorber mode-locking with dynamic gain saturation, (b) fast saturable absorber mode-locking, (c) mode-locking with slow saturable absorber without dynamic gain. Image regenerated from [24].

From Figure 5, the short net gain window in (a) and (b) leads to the formation of an ultrashort pulse. The dynamic gain condition in (a) is not observed in solid-state lasers but only in dye, semiconductor and colour-centre lasers. Hence, for some time, it was believed that a fast saturable absorber is required for passive mode-locking in solid-state lasers, such as the case in (b) where the gain is saturated to a constant level. However, mode-locking using slow saturable absorbers in Ti:sapphire (case (c)) was demonstrated [25], revealing that mode-locking in solid-state laser is possible with a slow saturable absorber. The explanation for the formation of pulse is less intuitive in the case of (c) since the net gain window persists after the pulse is formed. In the picosecond regime, the pulse is stabilised as the pulse is constantly pushed back in time by the absorber, merging with any noises that is caused by the remaining net gain. In the femtosecond regime, the pulse shaping mechanism is guided by soliton effect using the interplay of dispersion and self-phase modulation [26]. Soliton pulse shaping is also applicable to fast saturable absorber, which can lead to pulses two times shorter than pulses without soliton formation [27].

The recovery time of saturable absorber which typically occurs in the timescales of femtoseconds, cannot be measured directly by conventional detectors. The pump-probe experiment is a useful technique to measure the recovery time of a saturable absorber indirectly. The pump beam induces photoexcitation in the saturable absorber and after a time delay, the changes that occurred are detected by the probe beam. By tuning the time delay between the pump and probe beams, the changes in intensity of the pump beam can be measured. It is possible to obtain the recovery time from the relationship of the change in intensity as a function of time delay using a bi-exponential model:

$$y(t) = y_0 + Ae^{\frac{t-t_0}{\tau_1}} + Be^{\frac{t-t_0}{\tau_2}} \quad (8)$$

where y_0 and t_0 are offsets of the intensity (y) and time delay (t) respectively. A and B are the amplitudes while τ_1 and τ_2 are the recovery times of the fast and slow component respectively.

The time resolution of the measurement is dependent on the pulse duration of the pump and probe pulses. In the femtosecond pulse regime, two recovery times will be observed. The modulation depth of the fast component stabilises femtosecond lasers [28] and governs the steady state pulse duration of mode-locking. The slow component does not infer that the pulse duration will be longer, in fact as discussed earlier, pulse duration shorter than the recovery time is possible and the slow component actually helps to self-start mode-locking. In the picosecond regime, the recovery time only has one component with the fast component usually not observed [24].

2.2.2.2 *Types of Saturable Absorbers*

One of the earliest demonstration of passive mode-locking used dye laser. The saturable absorber and the active medium were mixed to form a composite medium dye laser generating 0.5 -1 ps pulses [29]. However, that method was superseded by other mode-locking technology since the handling and maintaining of dye solution are not straightforward. In particular, artificial mode-locking such as additive pulse mode-locking (APM) and Kerr lens mode-locking (KLM) were developed. Due to limitations in cavity design for artificial saturable absorbers, semiconductor saturable absorber mirror (SESAM) was instead commercially used to start and sustain passive mode-locking. Meanwhile, with the recent development in nanotechnology, a new group of carbon allotropes namely carbon nanotube (CNT) and graphene were successfully engineered and exhibit superior saturable absorber properties, which could potentially replace SESAM.

SESAM

Semiconductor saturable absorber mirror (SESAM) is made of two main parts: the semiconductor quantum well and the Bragg mirror. Depending on the choice of semiconductor used, a range of emission wavelength from 400 nm up to 2.5 μm could be tailored to specific needs. Typically, for emission in the mid-infrared, GaInAsSb-based materials are used [24]. The Bragg mirror is made of material that has a high bandgap to ensure that no absorption occurs at the mirror. SESAM is a slow saturable absorber with recovery time in the range of picoseconds, which exhibit gain and loss similar to Figure 5(c) [28]. The recovery time, absorption wavelength, saturation intensity and fluence can be controlled by manipulating the design and growth parameters of SESAM. This will require complex, expensive and time-consuming fabrication processes such as molecular beam epitaxy (MBE), metal organic phase vapor epitaxy and metal organic chemical vapour deposition. In addition to complying to stringent fabrication processes, high energy heavy-ion implantation is often

employed to induce defects in SESAM to reduce the recovery time [30]. Although the design of SESAM allows flexibility in terms of saturable absorption parameters, this usually required complex fabrication. Hence, there is a need to explore other possible materials as saturable absorber such as CNT and graphene.

CNT

Carbon nanotube (CNT) is a 1D carbon nanostructure and often visualised as a rolled up sheet of graphene, with nanoscale diameter and micrometer in length. Compared to SESAM, CNT possesses more advantages. Firstly, CNT has a faster recovery time than SESAM, with recovery time less than 1 ps was reported by [31] and able to support generation of very short pulse, down to 66 fs [32]. Secondly, the fabrication process of CNT saturable absorber is much simpler using combination of wet chemistry, organic solvents and appropriate host polymers to grow the CNT and spin-coat the nanostructure onto desired optical devices [33]. Thirdly, CNT offers flexibility in terms of wavelength operation and modulation depth. By varying the diameter and chirality of CNT saturable absorber, the operating wavelength and bandwidth can be tuned [34] and by varying the thickness of the CNT layer, the modulation depth of the saturable absorber can be scaled [35]. However, the tunability of the absorption band by having a wide distribution in tube diameters leads to additional loss due to some tubes which are off-resonance at that particular wavelength [36]. However, CNT exhibits saturable absorption from the visible wavelength up to 2.1 μm [37]. There is still a gap to be fulfilled for saturable absorber beyond that wavelength.

Graphene

Ever since the first demonstration of mode-locking using monolayer graphene [38], graphene has been widely used for passive mode-locking [6, 38, 39]. Previous saturable absorbers such as SESAM and CNT has limited bandwidth operation, whereas graphene exhibits saturable absorption properties from 0.8 μm [40] to 3.0 μm [41]. Coupled with its ability to be easily adapted to technology previously designed for CNT [42], graphene is the preferred saturable absorber for mode-locking in the mid-infrared region. Since graphene is the major focus of this thesis, the properties of graphene as a saturable absorber will be elaborated in detail in a dedicated section (refer Section 2.3).

2.2.3 Dispersion Compensation

Besides saturable absorber, another parameter that is important for mode-locking is dispersion. The dependency of phase shift φ on frequency ω is termed dispersion and occurs when a pulse travels through a medium which has wavelength-dependent refractive index. Since a mode-locked laser has a broad frequency spectrum, phase shifts due to dispersion effect will broaden the mode-locked pulse. The frequency-dependent phase shift can be expressed in a Taylor series around the centre frequency ω_0 of the pulse [24]:

$$\varphi(\omega) = \varphi_0 + \frac{\partial \varphi}{\partial \omega} (\omega - \omega_0) + \frac{1}{2} \frac{\partial^2 \varphi}{\partial \omega^2} (\omega - \omega_0)^2 + \frac{1}{6} \frac{\partial^3 \varphi}{\partial \omega^3} (\omega - \omega_0)^3 + \dots \quad (9)$$

The first-order dispersion $\frac{\partial \varphi}{\partial \omega}$, which is the group delay does not modify the pulse shape but the second-order (group delay dispersion or GDD) and higher-order phase shifts tend to affect the temporal shape of the pulse, especially in the femtosecond regime. In most cases, GDD can be ignored for pulse duration above 10 ps.

The net GDD for a cavity is typically positive or sometimes called normal due to dispersion in the laser gain medium and other components in the cavity. However, for soliton pulse formation, a negative GDD is often preferred. There are a number of ways to control and compensate the cavity's net dispersion. Examples are the used of prism pairs and chirped mirrors. Prism pairs technique allow the dispersion to be controlled by adjusting the relative distance between the two prisms. On the other hand, chirped mirrors are dielectric mirrors with specially engineered surface layer to introduce a specific dispersion into the cavity. Chirped mirrors can be designed to compensate third-order dispersion and often use in combination with prism pairs.

2.3 Graphene as a Saturable Absorber

2.3.1 Properties of Graphene

Graphene is a 2D nanostructure made up of a single layer of carbon, making it the thinnest known material. Despite being only one atom thick, it is also the strongest known material [43] due to localized electrons with sp^2 -bonds between the hexagonally arranged carbons. Unlike any other material, graphene has no bandgap. Delocalised electrons near the overlap of the conduction band and valence band at the six corners of the Brillouin zone, known as the Dirac points [44] leads to graphene's unique optical and electronic properties [45]. Any excitation will lead to an electron-hole pair, providing graphene a wide operational wavelength range extending into mid-infrared region [39]. Coupled with its high absorption of incident light per layer [46] and ultrafast carrier dynamics [47], graphene is an attractive choice of saturable absorber for mode-locking in the mid-infrared. Important parameters of a saturable absorber that need to be considered when designing a laser are its recovery time and nonlinear optical properties including modulation depth and saturation fluence.

2.3.1.1 Nonlinear Optical Properties

The maximum change in absorption that can be induced by the incident light is defined as the modulation depth and pristine single layer graphene has modulation depth of 65.9 % [48]. Experiments have shown that by increasing the number of layers of graphene, the saturation intensity increases whereas the modulation depth decreases due to defect-induced non-saturable loss and scattering [48, 49].

The saturation fluence is defined as the fluence (energy per unit area) required to reduce the absorption to $1/e$ of its initial value. In other words, a higher saturation intensity would require more incident light to reach saturation. Saturation fluence J_{sat} can be estimated using this relation:

$$J_{sat}(\mu m/cm^2) = \frac{E_{int}}{A} \quad (10)$$

where E_{int} is the intracavity pulse energy and A is the beam spot size.

2.3.1.2 Recovery Time

The first attempt to characterise graphene relaxation dynamics using pump-probe technique found that graphene has a fast relaxation time in the range of 70-120 fs while the slow relaxation time is in the range of 0.4-1.7 ps [47]. The fast component depends on carrier thermalization by electron-electron interaction while the slow component is attributed to the cooling of carrier distribution by electron-phonon interaction [47]. The fast component was found to have a larger value when the number of graphene layers increases [48]. These are typical timescales of graphene saturable absorber reported in near-infrared pump-probe experiments [50] whereas these timescales in the mid-infrared are not yet widely established.

2.3.2 Fabrication and Characterisation of Graphene

Graphene was first obtained via mechanical exfoliation [51] or also known as the *Scotch tape method*. By using a simple Scotch tape, the graphene layers are repeatedly peeled from a highly ordered graphite crystal until atomic-layer thin of graphene is achieved and then transferred onto a substrate while preserving the graphene's hexagonal honey-comb structure. Although this method is simple and straightforward, it is difficult to regulate the size, shape and thickness of the graphene, which is unattractive for commercial exploitation. Other methods have been developed since then to produce graphene, such as epitaxial growth on silicon carbide, chemical vapour deposition (CVD) and wet chemical methods. Of all these available methods, CVD graphene is commonly used for transferring graphene onto other substrates. In this approach, the graphene is grown on the surface of transition metal such as nickel and copper as substrates. The surface of the substrate is subjected to temperature up to 1000 °C before being exposed to a mixture of gases such as hydrogen, argon and methane. The carbon from the cracked methane diffuses into the metal and this is followed by rapid cooling to precipitate out graphene on the surface [50]. The CVD graphene can be transferred easily on to desired substrate by applying a polymer structural support to keep the structural integrity of the graphene before etching the underlying metal substrate away.

Raman Spectroscopy

It is difficult to visually identify monolayer graphene on a Si substrate. Typically, a thin layer of SiO₂ (~100 nm or 300 nm) is added on the surface of the Si substrate to improve the contrast and visibility of graphene [52]. Another common method to identify graphene is via Raman spectroscopy [53-55]. Light can be scattered inelastically whereby the incident photon and scattered photon have different frequencies. Raman scattering is manifested in this inelastic scattering of light. At different atomic position within the vibrational mode displacements of the atom, the polarisability of the atom is different. These characteristic vibrational modes are known as normal modes and are attributed to chemical and structural properties of materials. Since every material has its own fingerprint set of normal modes, Raman spectroscopy can be used to probe materials properties in detail [56]. A small change in geometric and chemical bonding within the sample will produce a significant change in its Raman spectrum. For example, graphene, diamond and graphite are carbon-based material which differs in their arrangements of carbon atoms and the type of bonding between them. The Raman technique can distinguish these materials quickly and non-invasively without much sample preparation. For this experiment, the Raman technique is sufficient to determine the quality of the transferred graphene and to determine the number of graphene layers.

A typical Raman spectrum of graphene has 2 principle peaks called G and G' band. Occasionally, a third band called the D band is present when defect is present in the graphene. The D, G and G' band located at approximately 1350 cm⁻¹, 1582 cm⁻¹ and 2700 cm⁻¹ respectively [55] as shown in Figure 6.

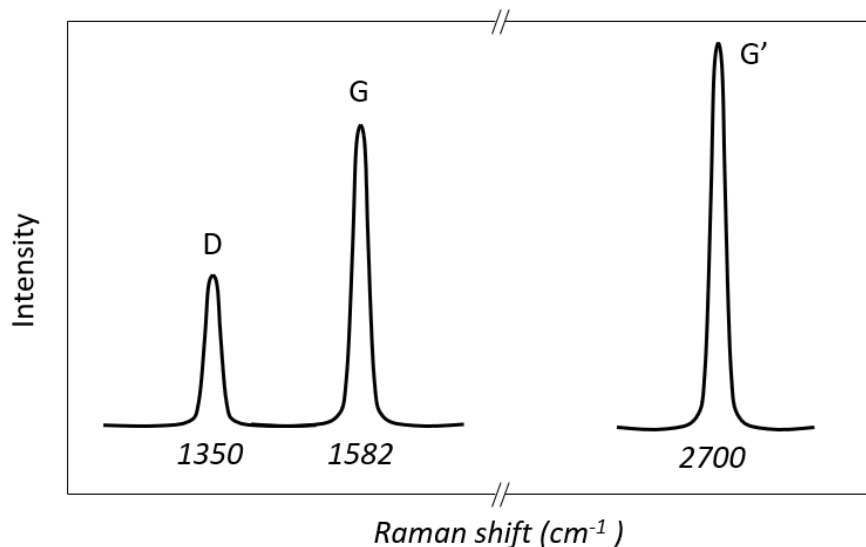


Figure 6. A typical Raman spectrum of monolayer graphene with D, G and G' band located at approximately 1350 cm⁻¹, 1582 cm⁻¹ and 2700 cm⁻¹ respectively.

The D band (~1350 cm⁻¹) [55] otherwise known as the defect or the disorder band, exists due to the presence of defect. In a defect-free graphene, this band is suppressed whereas if the D band is significant, the graphene has a lot of defects. The level of

defect or disorder can be quantified by calculating the ratio of the intensity of D band to intensity of G band (I_D/I_G) [57].

The G band located at around 1582 cm^{-1} [55] is associated with the in-plane vibrational mode due to the stretching of C-C bond in graphene. Stacking another layer of graphene on top of a layer of graphene will induce strain effect on the bonding which will shift the position of the G band. The position shifts towards lower energy as the number of graphene layer increases. Hence, the position of G band is sometimes used to determine the number of layer of graphene [57].

The G' band which occur at approximately 2700 cm^{-1} [55] originates from two-phonon lattice vibrational process and sometimes is denoted as 2D band since it is a second order overtone of the D band. However, unlike its D band counterpart, G' band does not characterise defect, but it represents the number of graphene layers. The shape of G' band tends to be broader and blue-shifted as the number of graphene layer increases [57].

The number of layers of graphene can be estimated by the ratio of peak intensity of G band to G' band ($I_G/I_{G'}$) [58]. The intensity of G and G' band varies as the number of graphene changes. The intensity of G band increases whereas the intensity of G' band decreases and broadens as the graphene number increases.

Chapter 3: Fabrication and Characterisation Methods for Graphene Saturable Absorber Mirrors

In this work, the graphene saturable absorber mirrors are fabricated by transferring graphene onto different kinds of mirrors: silver, sapphire and chirped mirrors. Subsequent characterisation using Raman spectroscopy is conducted to analyse the transferred graphene and followed by pump-probe experiment to measure the recovery times of the graphene saturable absorber mirrors. These graphene mirrors will then be integrated into the laser cavity to generate mode-locked pulses.

In this chapter, the focus will be on the material physics of graphene. The graphene transfer process will be discussed, and the characterisation is limited to Raman spectroscopy in this chapter. The characterisation of the recovery times will be elaborated in the next chapter, Chapter 4.

3.1 Graphene Transfer

CVD-grown graphene was chosen for this work because it is available commercially and its subsequent transfer process is widely studied. The large area synthesis of CVD graphene allows the graphene sheet to be cut into several small pieces and transferred onto arbitrary substrates. Since CVD-graphene is grown on a metal substrate, transfer process is necessary to transfer the graphene from the metal substrate on to a desired substrate. The most popular transfer method is polymer-mediated transfer, using polymethyl metacrylate (PMMA) as a temporary support while the metal substrate is etched away [58]. When the graphene is transferred onto the substrate, the polymer support is then removed. A direct transfer without polymer support is also possible and has been reported [59], which follow similar steps as polymer-mediated transfer, skipping the steps involving PMMA. Although this method is reported to be quicker and clean from PMMA residue, when tried in our lab, the ultrathin graphene without any supportive layer was very difficult to be handled as it was prone to ripping and broke apart easily.

In this work, polymer-mediated transfer was employed to transfer monolayer CVD-graphene grown on Cu foil on to different substrates: Si wafer, silver mirror, sapphire mirrors and dielectric mirrors. Different types of PMMA were also tested to determine the most suitable choice of PMMA and the influence of other parameters such as etching time and post-transfer baking time were also investigated. The influence of these parameters is discussed in Appendix. Overall, at least ten transfer attempts were performed using Si wafer as a dummy substrate, to determine the best transfer

parameters before attempting to transfer graphene onto a silver mirror, 2 sapphire mirrors and 2 chirped mirrors. The result of all the transfer attempts on Si wafer are presented in Appendix Table 3. The summary of attempts to transfer graphene onto Si wafer, by changing different kind of parameters. Table 3, whereas the result of the transferred graphene onto the mirrors are presented in Section 3.2. The transfer of graphene and the subsequent characterisations were performed at NTNU Nanolab clean room facility.

Step one: Spin-coating of PMMA

The graphene used in this project is a monolayer CVD graphene grown on copper foil with dimensions of 60 mm x 40 mm bought from Graphenea. The graphene sheet was carefully cut using a sharp scissor into a square with sides of approximately 1 cm. The remaining graphene sheet was stored in a vacuum container to minimise the oxidation of the copper foil.

Monolayer graphene is very thin rendering it prone to damage during the transfer process. A layer of polymer, Polymethyl metacrylate (PMMA) A12 (molecular weight 200 000 gmol⁻¹, 12% by volume dissolved in anisole) was spin-coated onto the graphene film to act as a sacrificial protective layer, before the transfer process.

The small graphene piece was fastened onto a Si wafer using one-sided kapton tape covering the graphene area as little as possible. This is to ensure that the lightweight graphene piece will not be flung out during the spinning process and preventing the PMMA from seeping into the bottom side of the graphene. A drop of PMMA was deposited onto the exposed graphene and the PMMA was spin-coated at a speed of 6000 rpm, acceleration of 2000 rpms⁻¹ for 2 minutes. This was followed by soft-baking on a hotplate at 105°C for 10 minutes to evaporate any solvent residue and to harden the resist. To make the structure more rigid, a frame of blue tape was fixed onto the PMMA surface so that the structure would not fold over itself, keeping it stretched out. The blue tape could be easily removed at the end of the transfer process.

Step two: Removal of Residual Graphene

Although graphene is intentionally grown on the top side of the copper substrate but due to the synthesis process, CVD graphene tend to have residual graphene grown on the back-side of the copper substrate as well. The back-side graphene is usually high in defect and was not needed and removed using oxygen plasma cleaner (50% oxygen flow, 50% power) for 12s. Short cleaning time is preferable to avoid further curing of the PMMA. Other method of removing the bottom layer graphene has been suggested such as using nitric acid [60]. However, this method is slightly risky because prolonged contact with the strong nitric acid may etch through the copper layer, reaching the top layer graphene.

Step three: Etching of Copper substrate

The next step is to remove the copper substrate layer. This was done via chemical etching. The etchant used was 0.1 M ammonium persulfate (APS), prepared by adding 200 ml of deionised water to 6 g of APS powder. PMMA/graphene/Cu film was placed in the etchant bath with the Cu surface touching the etchant for about 3-4 hours or until the copper layer disappears. By using a magnetic stirrer to stir the sample at 50 rpm, the etching time could be reduced to 2 hours. APS was chosen because it is strong enough to etch away the Cu layer but not graphene, leaving a transparent layer of PMMA/graphene floating on the solution. Although FeCl_3 is typically used to etch Cu [61, 62] due to its etching efficiency [63], it severely weakens the grain boundaries between crystallites in CVD-graphene, than compared to APS [64]. HNO_3 [65] and HCl [63] are also adept at etching Cu but the H_2 gas bubbles formed during these etching process could cause cracking in the graphene film and etching due to HCl releases poisonous gas [63]. Residual etching solution on the PMMA/graphene film was cleaned by transferring the film from a beaker filled with deionised water to another beaker with deionised water using a clean glass slide. This step was repeated at least 3 times to minimise residual etching solution contaminating the sample.

Step four: Transfer onto Desired Substrate

The graphene was transferred onto the target substrate by scooping up the PMMA/graphene film using the target substrate. A good transfer not only produce graphene free from contamination but also continuous without any cracks. Generally, when PMMA/graphene film is scooped up from the water using the target substrate, graphene layer does not make full contact with the surface of target substrate due to water trapped between the graphene layer and the surface of target substrate. Consequently, when the PMMA support is removed later on, these unattached regions break and form cracks [66]. To remove the water, after transferring the PMMA/graphene film on to the target substrate, the sample was left to dry at an inclined angle in ambient condition overnight. Water surface tension and gravity will drag the film into contact with the substrate. As the film is not completely smooth (since the growth of graphene follows the roughness of the surface of the copper substrate), some water may still be trapped and not completely removed. The sample was soft-baked on a hotplate to evaporate this trapped water at temperature of 80°C , lower than the recommended baking temperature of 150°C [66] to avoid further curing of the PMMA. To compensate for the lower temperature, the baking time was lengthened from the recommended time of 15 minutes [66] to 1 hour. If the target substrate is a (silver, sapphire or chirped) mirror, the graphene/mirror was baked for 4 hours instead of 1 hour since mirror is thicker and has different thermal conductivity compared to Si wafer. Another way to create smooth contact between the graphene film and substrate is by increasing the hydrophilicity of the substrate surface, to spread the water more evenly during transfer [66]. The target substrate surface was treated using oxygen plasma cleaner (50% oxygen flow, 50% power) for 1 minute. Oxygen plasma treatment not only made the substrate surface more hydrophilic but also remove contaminants on the substrate before the transfer.

Step five: Removal of PMMA

Once the graphene is adhered onto the substrate, the protective layer is no longer needed. The PMMA coating and the blue frame were removed by placing the sample in an acetone bath. Thicker and harder PMMA layer is more difficult to be removed and most of the time cannot be removed completely, leaving some PMMA residues on the graphene [67]. After immersing the sample in the acetone bath for 4 hours, the sample was rinsed with isopropanol and left to dry overnight.

Multilayer Graphene Transfer

To obtain double layer graphene on the same substrate, the entire process from step one to five were repeated. In principle, this process can be repeated multiple times to get multiple layers of graphene on the same substrate.

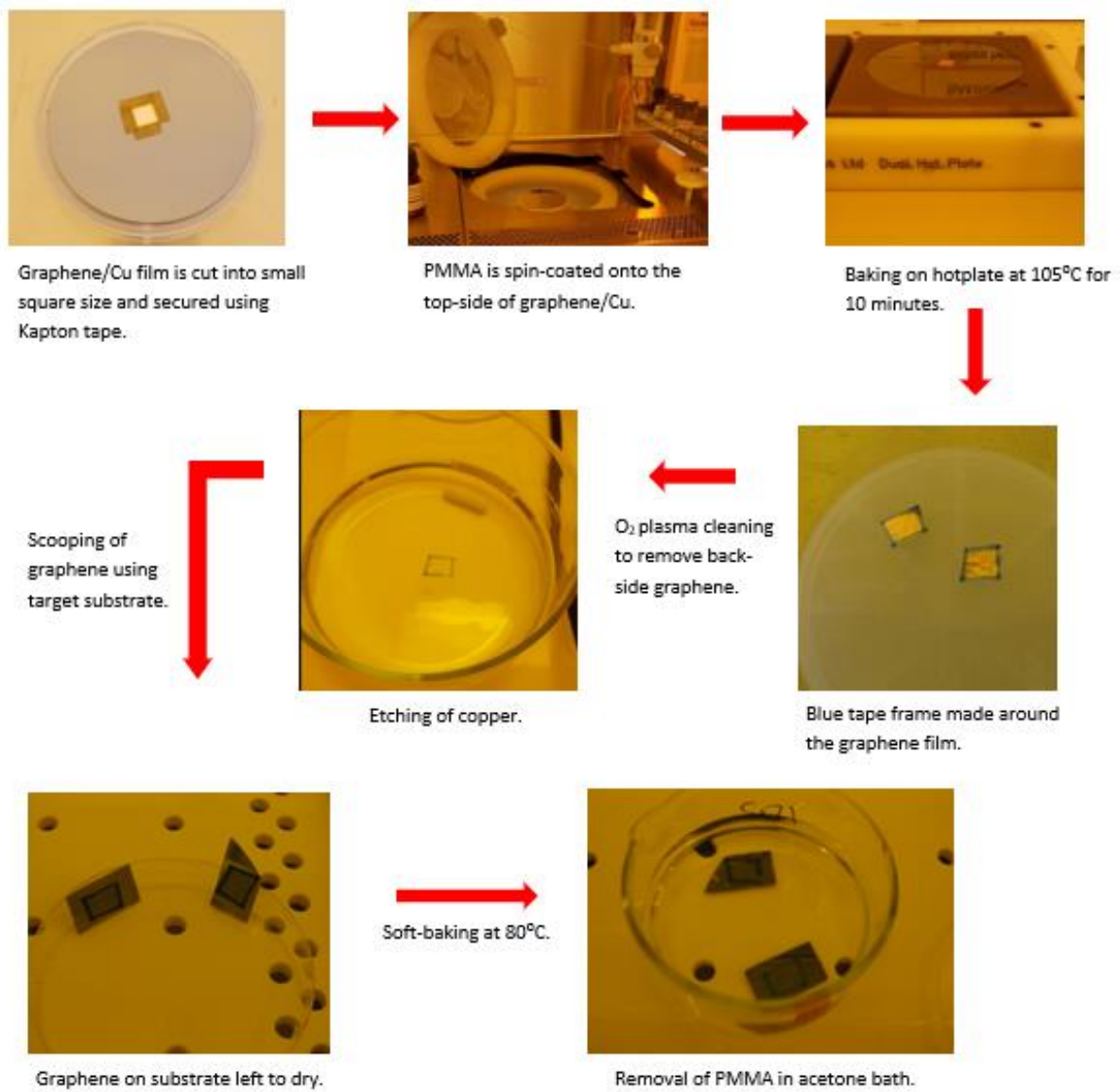


Figure 7. An overview of PMMA-mediated transfer of graphene. The substrate used is Si wafer.

3.2 Raman Spectroscopy

The transferred graphene was characterised using Raman spectroscopy to check the level of defect and the number of layers of graphene. The Raman spectrum of graphene has 3 significant peaks: D, G and G' band located at approximately 1350 cm^{-1} , 1582 cm^{-1} and 2700 cm^{-1} respectively [55]. The level of defect or disorder can be quantified from the ratio of the intensity of D band to the intensity of G band (I_D/I_G) [57] with value 0.05-0.3 deemed as acceptable [58]. The number of layers of graphene can be estimated by the ratio of peak intensity of G band to G' band ($I_G/I_{G'}$). 1-2 layer graphene has $I_G/I_{G'}$ of 0.5-1 respectively [58].

CVD Graphene

The as-bought graphene film was characterised using Raman spectroscopy to check the level of defect on the top-side and back-side of the film. The Raman spectrum of the top-side is shown in Figure 8, whereas the spectrum of the back-side is shown in Appendix (Figure 29). As expected, the back-side graphene has a significant D peak indicating high defect, whereas this D peak is suppressed on the top-side graphene. The top-side, which is assumed to be monolayer, has $I_G/I_{G'}$ of 0.581. If the transferred graphene has a higher $I_G/I_{G'}$ value than 0.581, then the number of graphene layer is more than one.

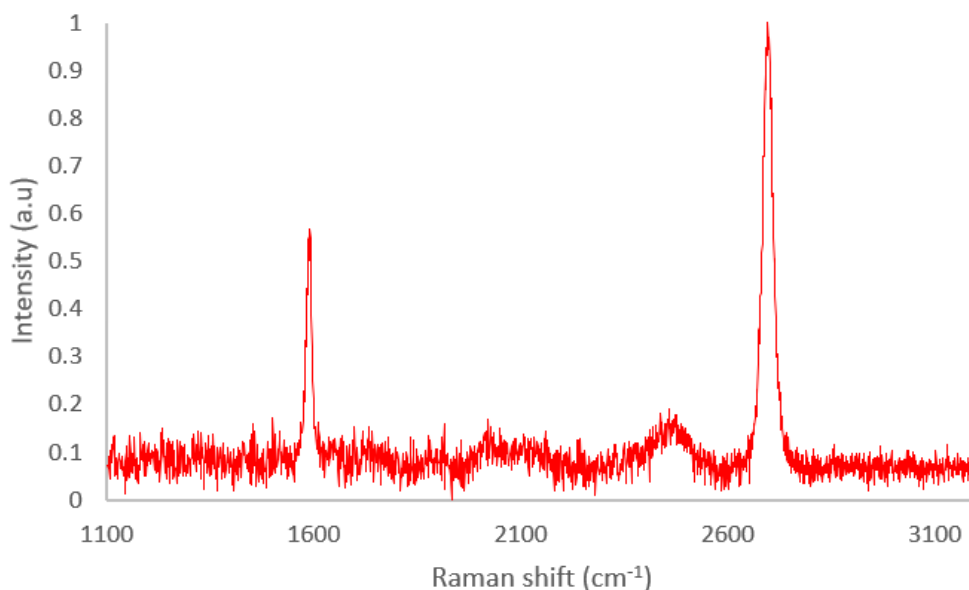


Figure 8. Raman spectrum of the as-bought CVD graphene (top-side) with G and G' peaks at 1590 cm^{-1} and 2698 cm^{-1} respectively. The D band is not present.

Graphene on Silver (Ag) Mirror (GAM)

The graphene on silver mirror is denoted as GAM. The Raman spectrum of graphene/mirror as shown in Figure 9(a) has sharp G (1585 cm^{-1}) and G' (2678 cm^{-1}) bands confirming that graphene is present, whereas the weak D (1343 cm^{-1}) band indicates the presence of defect. The level of defect, $I_D/I_G = 0.227$ is reasonable.

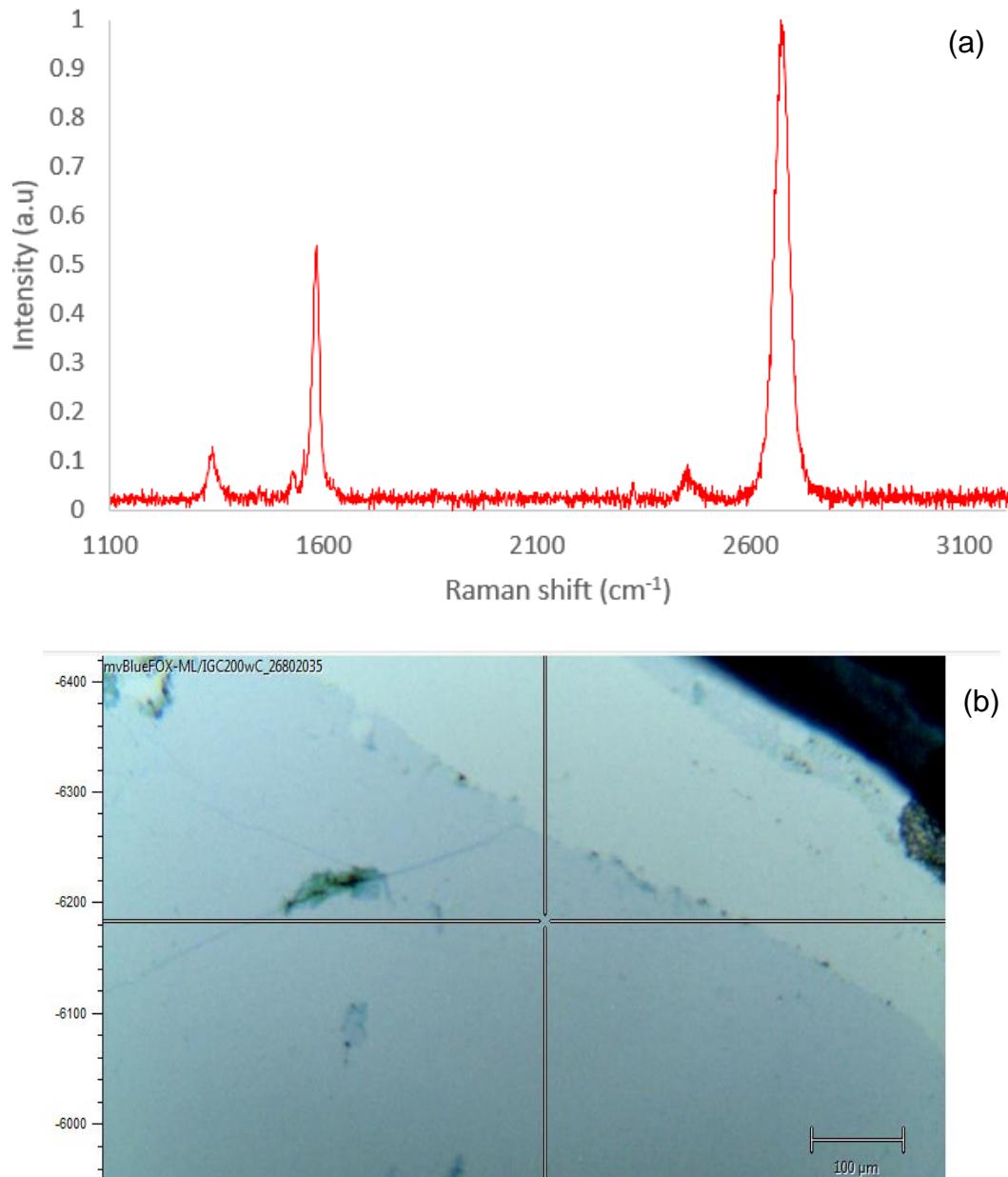


Figure 9. (a) Raman spectrum and (b) optical microscope image of single-layer graphene on Ag mirror (GAM).

Graphene on Two Sapphire Mirrors (GSM1 and GSM2)

Single-layer graphene was transferred onto one of the sapphire mirrors (denoted as GSM1) and two-layer graphene was transferred onto another sapphire mirror (GSM2). The defect peak is not obvious in GSM1 but reasonable defect, $I_D/I_G = 0.248$ was found on GSM2. Both has high G peak with GSM2 has $I_G/I_{G'}$ close to 1, confirming the presence of two-layer graphene.

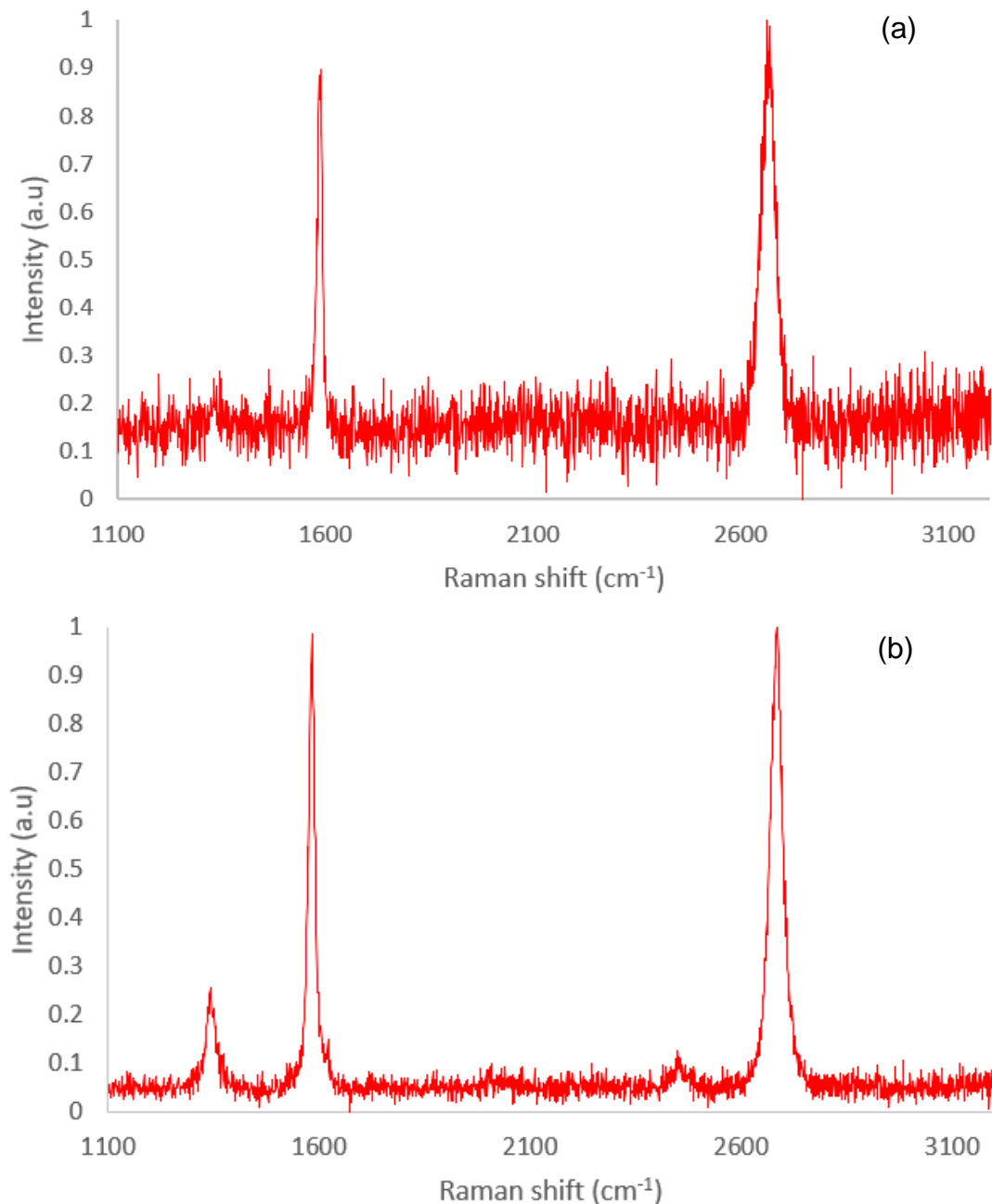


Figure 10. Raman spectra of (a) single-layer graphene on sapphire mirror 1 (GSM1) and (b) two-layer graphene on sapphire mirror 2 (GSM2).

Graphene on Two Chirped Mirrors (GCM1 and GCM2)

Single-layer and two-layer graphene were transferred onto two different chirped mirrors: chirped mirror 1 (GCM1) and chirped mirror 2 (GCM2). Both the chirped mirrors were designed for operation from 2.1 μm to 2.8 μm .

From Figure 11 and Figure 12, the intensity of G peak increases as the number of layer of graphene increases.

For GCM1, the area with single-layer graphene has $I_G/I_{G'} = 0.514$ and $I_D/I_G = 0.184$ and the area with double-layer graphene has $I_G/I_{G'} = 0.885$ and $I_D/I_G = 0.164$.

For GCM2, the defect peak was not observed. The area with single-layer graphene has $I_G/I_{G'} = 0.373$ and double-layer graphene has $I_G/I_{G'} = 0.769$.

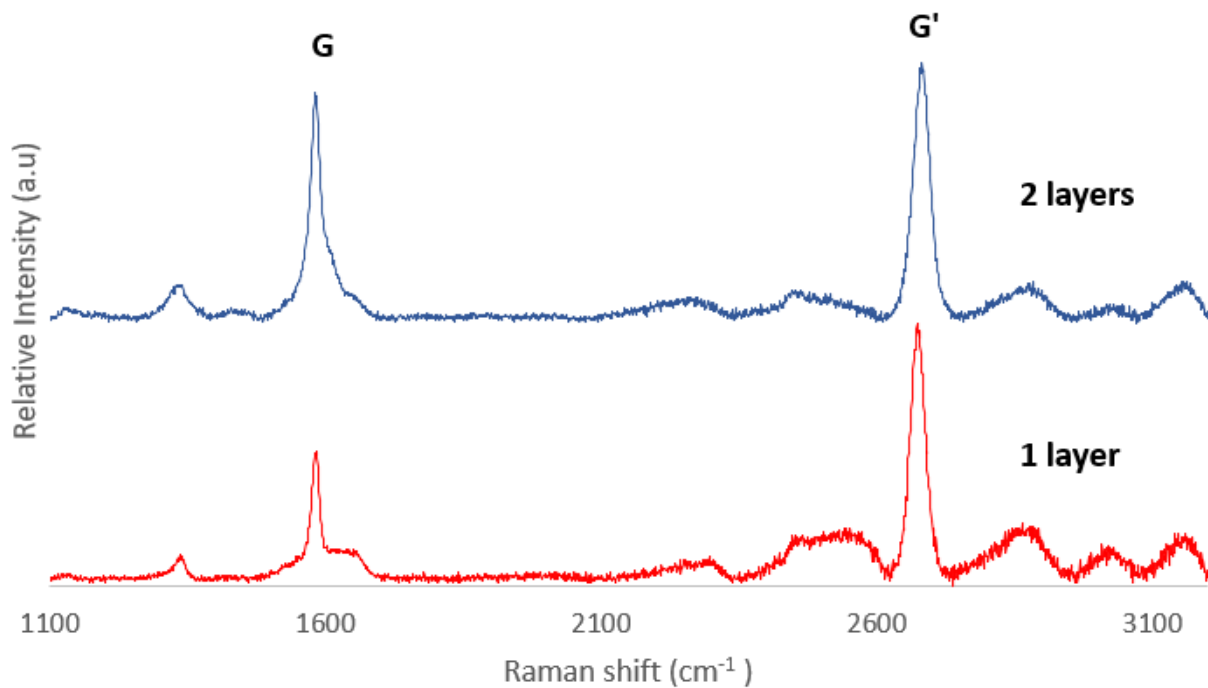


Figure 11. Raman spectra of single- and two-layer graphene on chirped mirror 1 (GCM1).

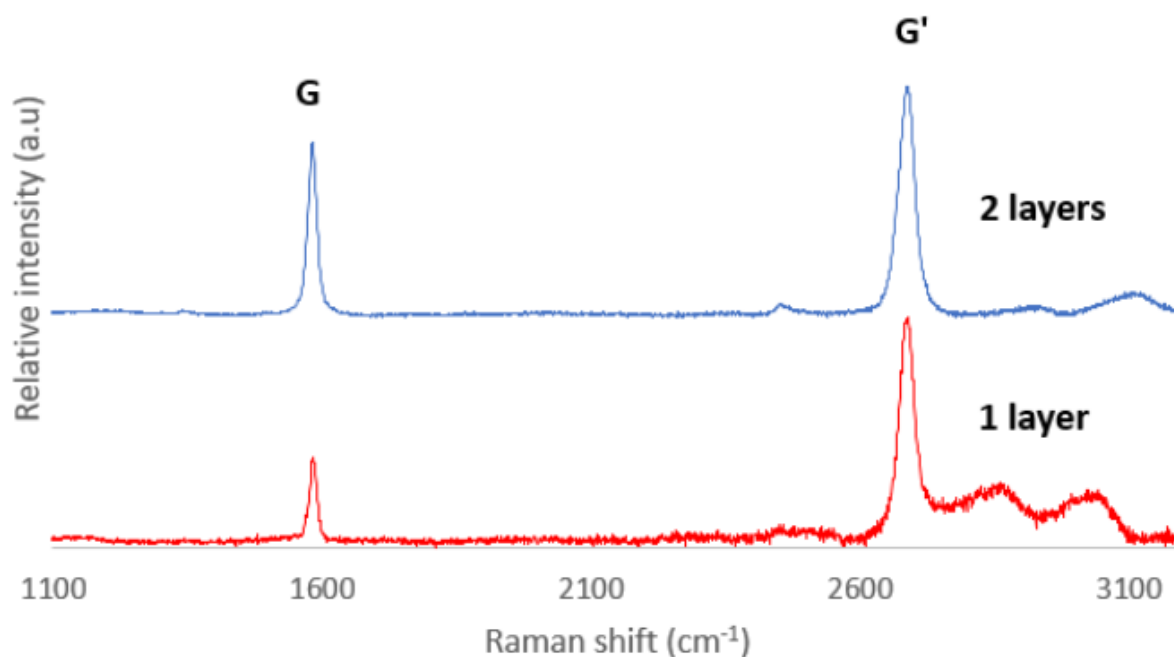


Figure 12. Raman spectra of single- and two-layer graphene on chirped mirror 2 (GCM2).

3.3 Discussion

Graphene was successfully transferred onto desired substrate mirrors with satisfactory defect level. The defect band is more prominent as the number of graphene layer increases, as shown in Figure 11. This may be attributed by the collective PMMA residue on the surface of the graphene from each layer of transferred graphene. Since two-layer graphene requires graphene to be transferred twice onto the mirror, it would require the use of PMMA twice. This is not efficient because during the first transfer, PMMA residue may not be removed completely before the addition of the second graphene onto the first layer graphene. Hence, it would be preferable to limit the use of PMMA to once only. A solution is this; when the first PMMA/graphene/Cu film is etched, instead of using the target substrate to scoop the graphene, a graphene/Cu film is used to scoop the etched graphene creating a stack of two layers of graphene with only one PMMA layer at the top (PMMA/1st graphene/2nd graphene/Cu). After the second etching of Cu, the target substrate is used to scoop the PMMA/1st graphene/2nd graphene film to create a stack of PMMA/1st graphene/2nd graphene/substrate. In principle, this can work on n -layers of graphene using PMMA once only. The transfer of two-layer graphene onto GSM2 was done using this method. Although two-layer graphene was successfully transferred, the graphene was not continuous and at some parts, the graphene was folded as shown in Figure 13. It was challenging to scoop-up the etched graphene using a flexible graphene/Cu film instead of a rigid substrate, which introduces these foldings. Hence, usually a compromise has

to be made. A 'cleaner' transfer (less PMMA residue) can be achieved but under the expense of less continuous and uneven transfer.

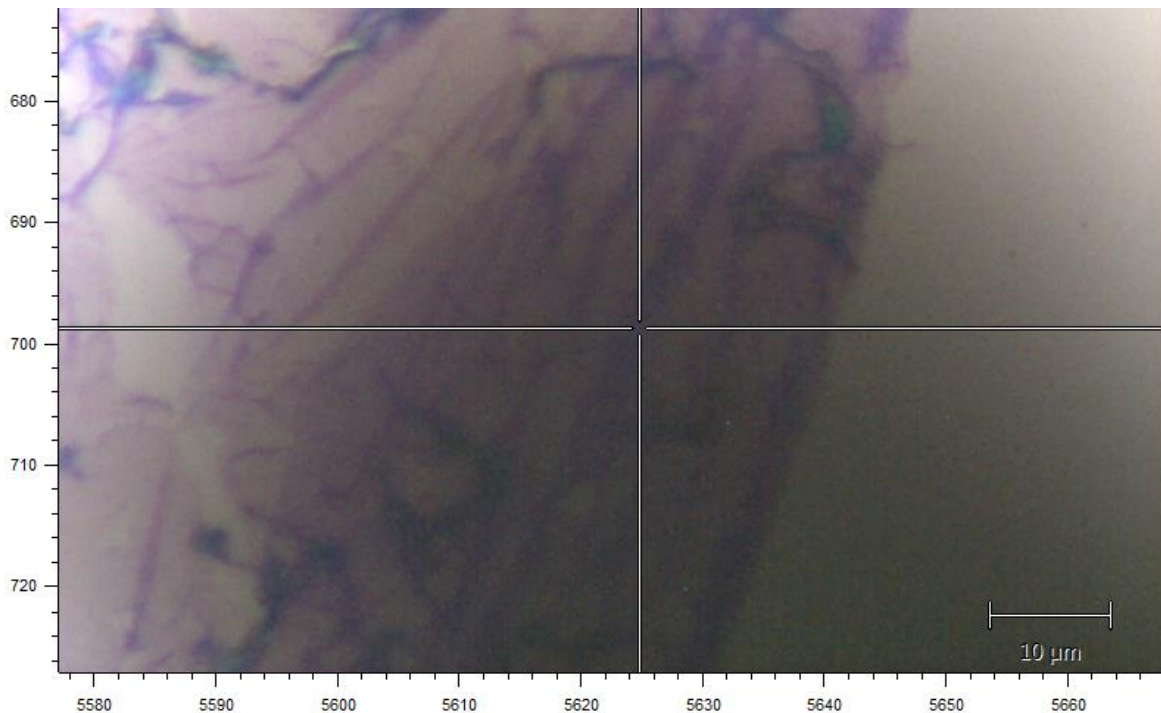


Figure 13. Raman microscope image of two-layer graphene on GSM2. The graphene is folded and not continuous with cracks on the left region of the image.

Another challenge in graphene transfer is the tiny gaps between graphene and the surface of the target substrate which cause an incomplete contact of graphene to substrate. Li et.al reported the use of an additional layer of PMMA to overcome this issue [68]. There are two main factors that caused these gaps. The first factor is the trapped water hindering full contact of graphene to substrate. This can be resolved by post-transfer baking to evaporate the trapped water. The second factor is because the surface of graphene itself is rough, following the surface of its metal substrate after metal reconstruction during CVD process. The pre-coated PMMA mimics the surface roughness of the graphene and since PMMA is a hard coating, the graphene does not relax when the PMMA is washed away. The introduction of a second layer of PMMA coated on top of the pre-coated PMMA will partially dissolve the pre-coated PMMA and allow redissolution of PMMA to occur which mechanically relax the underlying graphene and thus, improving the contact between graphene and the substrate [68].

Other suggested improvement would be to use a different type of PMMA removal that reduce PMMA residue on graphene. Compared to acetone, 1,2-dichloroethane is a much more efficient PMMA remover, as reported by [67].

To conclude, the transfer of graphene using PMMA-mediated technique, as described in Section 3.1, is an adequate method to transfer single- or double-layer graphene onto any mirror substrates, with satisfactory defect level.

Chapter 4: Experimental Setup

The recovery times of the graphene saturable absorber mirror were measured using pump-probe technique with a 2.4 μm femtosecond laser as well as a picosecond laser to compare the results between these two lasers. The ability of graphene chirped mirror as saturable absorber was also investigated using two different types of mode-locking cavities with Cr:ZnS as the gain medium.

4.1 Pump-Probe Experiment

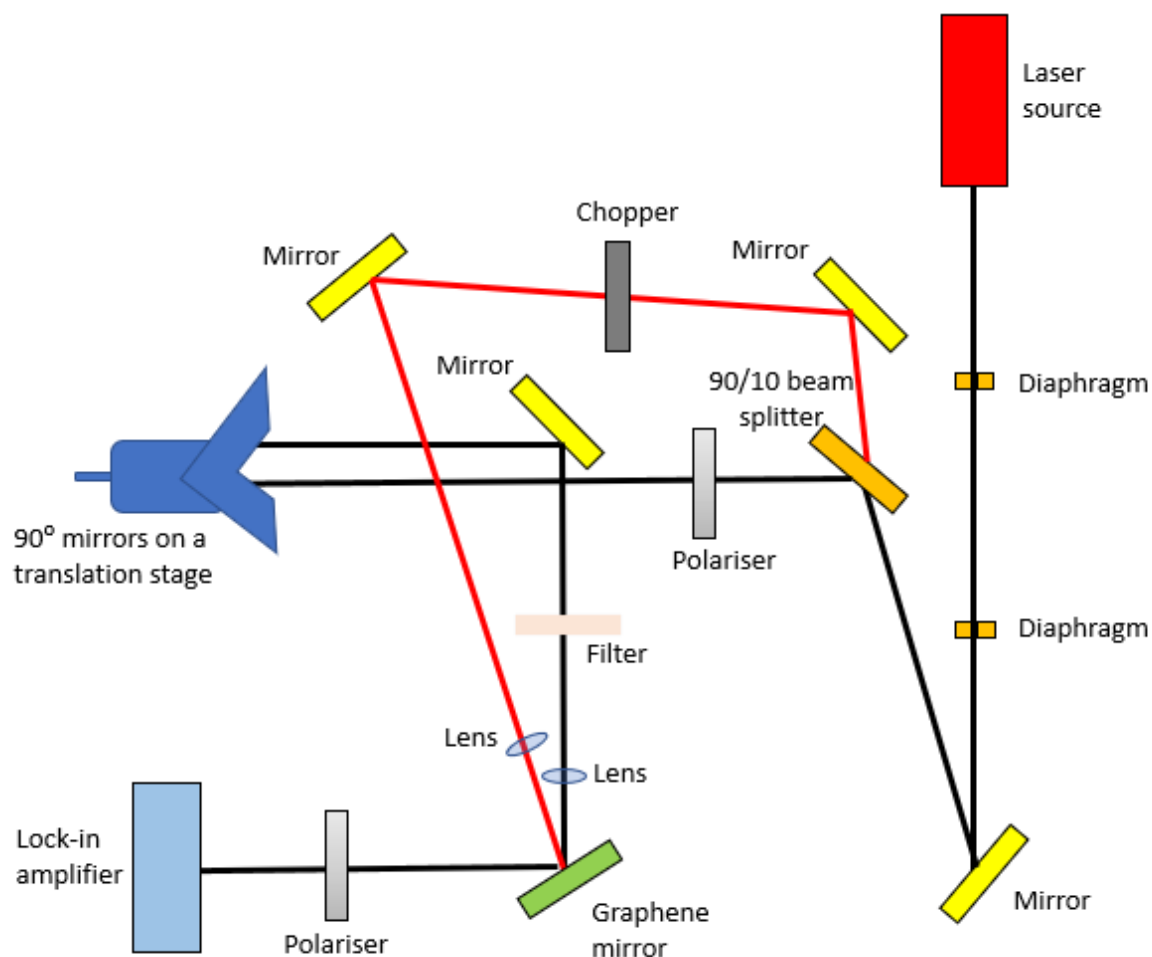


Figure 14. The pump-probe setup. The pump beam is coloured in red while the probe beam is coloured in black.

Figure 14 shows the setup of the pump-probe experiment to measure the recovery time of the graphene saturable absorber mirrors. The beam from the laser source was divided into two at the beam splitter with 90% of the beam passed through as the pump beam and 10% being reflected as the probe beam.

Both the pump and probe beams have a beam size of 30-40 μm when measured using a beam profiler. Also, the setup was arranged such that both the pump and probe beam travelled the same length before reaching the sample. Both beams travelled a distance of 60 cm before reaching the sample.

The pump beam was modulated by an optical chopper to 390 Hz before being focused onto the sample by a lens with focal length 25 mm.

On the other hand, after passing through the beam splitter, the probe beam would encounter a right-angled mirror on a translation stage. The stage could be moved to introduce time delay between the probe and pump beams. The probe beam was focused onto the sample by a lens with focal length of 10 mm. The probe beam reflected by the sample was detected by a lock-in amplifier.

A crossed polariser pair was used to filter out any parasitic interference from the pump component. The modulation frequency set by the chopper helped to distinguish noise from being amplified by the amplifier. A filter was fixed along the pump beam to avoid oversaturation on the detector.

By measuring the intensity of the reflected probe beam as a function of time delay, the recovery time could be determined using a bi-exponential decay model (equation (8)).

The laser source was a mode-locked Cr:ZnS laser, using the one-layer graphene on sapphire mirror 1 (GS1) as the saturable absorber. The setup of the laser is described in Section 4.2.2 and illustrated in Figure 19. By introducing a passive ZnS crystal before the output coupler, the dispersion of the cavity can be varied to deliver either picosecond or femtosecond pulses to the pump-probe system.

For slow saturable absorbers with recovery time in the range of picosecond such as SESAM and CNT, pulses with picosecond duration is sufficient. On the other hand, fast saturable absorber such as graphene require a femtosecond laser source.

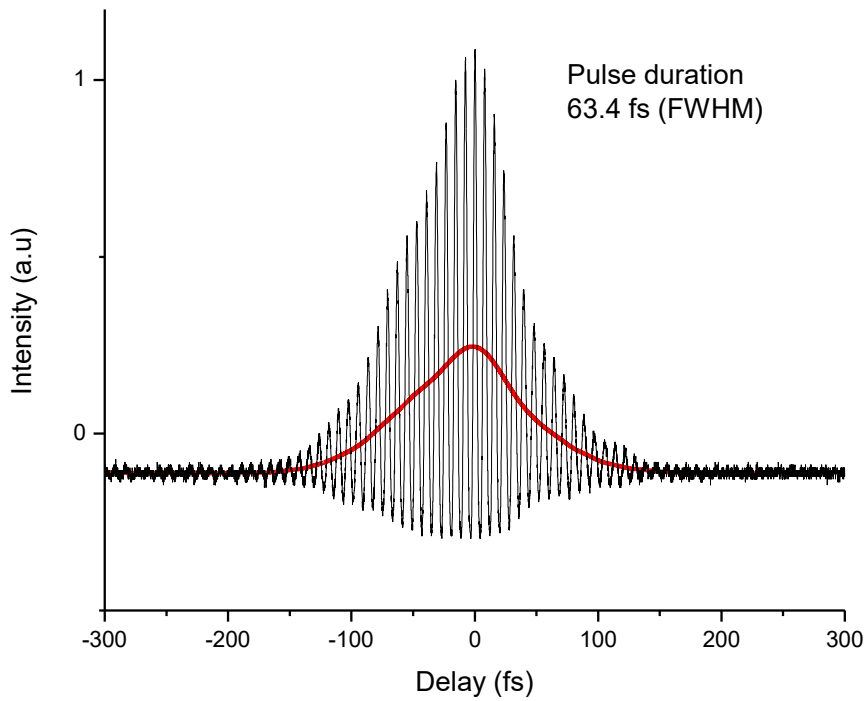


Figure 15. The autocorrelator measurement of the femtosecond mode-locked pulse source with FWHM (assuming sech shape) of 63.4 fs.

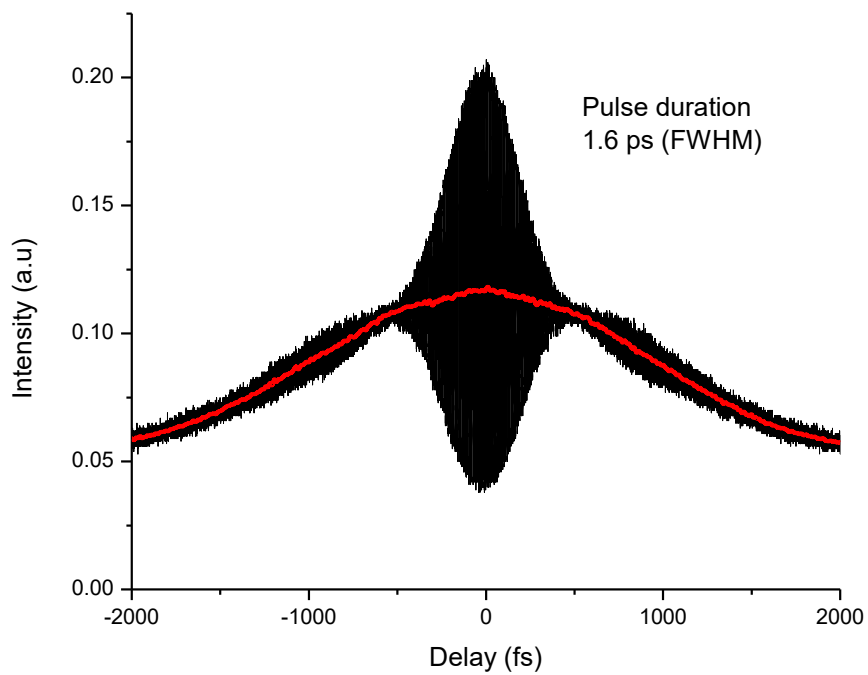


Figure 16. The autocorrelator measurement of the picosecond mode-locked pulse source with FWHM (assuming Gauss shape) of 1.6 ps.

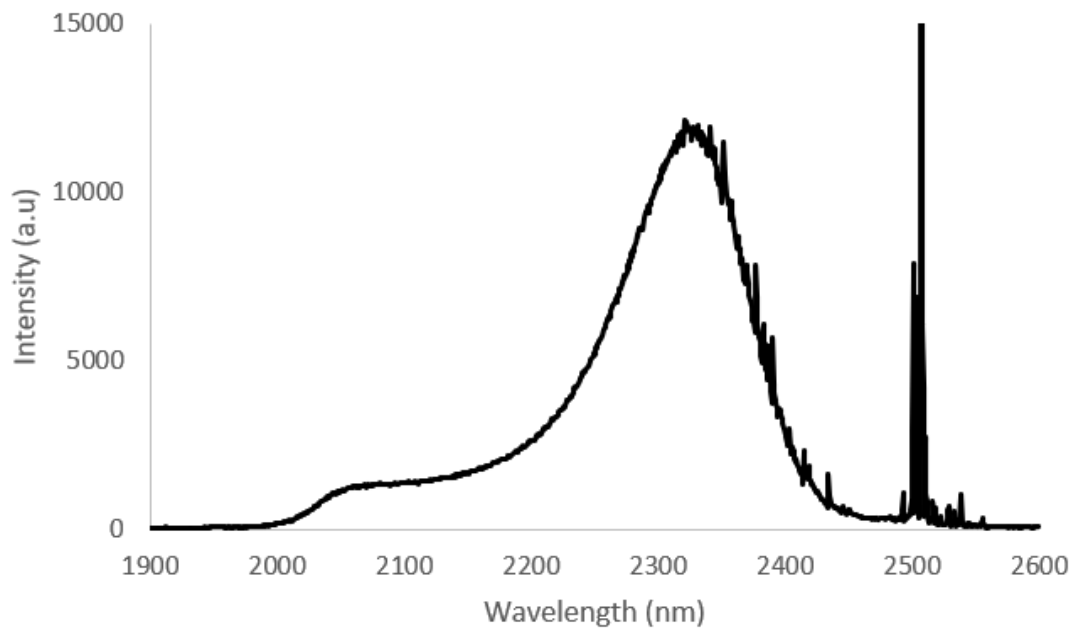


Figure 17. The spectrum of the mode-locked laser source.

In this work, the pump-probe technique was employed to measure the recovery times of a commercial SESAM and CNT using 1.6 ps mode-locked pulse operating at 2.35 μm and the recovery times of the graphene saturable absorber mirrors (GAM, GS2, GCM1 and GCM2) were measured using 64.3 fs mode-locked pulse operating at 2.35 μm .

4.2 Mode-Locking in Cr:ZnS Laser

Two types of mode-locked setup were used to test the mode-locking ability of the graphene saturable absorber mirror.

4.2.1 Standard Cr:ZnS Cavity

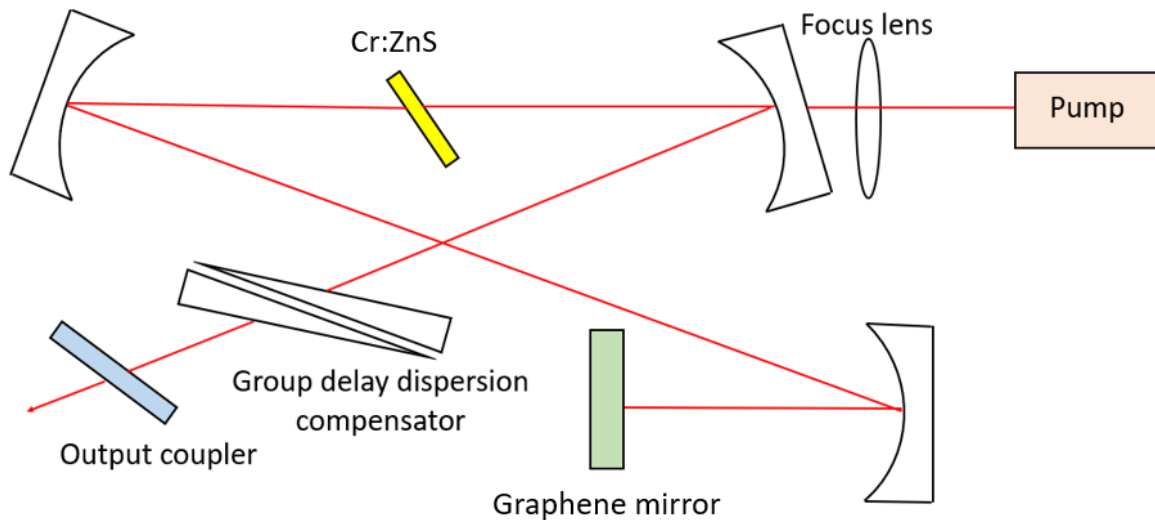


Figure 18. The standard Cr:ZnS cavity for mode-locking.

The saturable absorber tested in this standard Cr:ZnS cavity (Figure 18) was GCM1. The gain was pumped by an erbium-doped fiber laser emitting at $1.61 \mu\text{m}$. The cavity had a normal GDD due to the laser crystal and this was compensated by a pair of adjustable yttrium aluminium garnet (YAG) crystal.

At the 18% output coupler, the cavity could be connected to an optical spectrum analyser, autocorrelator and power meter to obtain the wavelength spectrum, pulse width and output power respectively.

4.2.2 Extended Cr:ZnS Cavity

The mode-locking ability of GCM1 was further investigated in an extended Cr:ZnS cavity to compare the performances of these two types of mode-locking. The source of laser in the pump-probe setup was based on this extended Cr:ZnS cavity using graphene on sapphire mirror (GS1) as the saturable absorber.

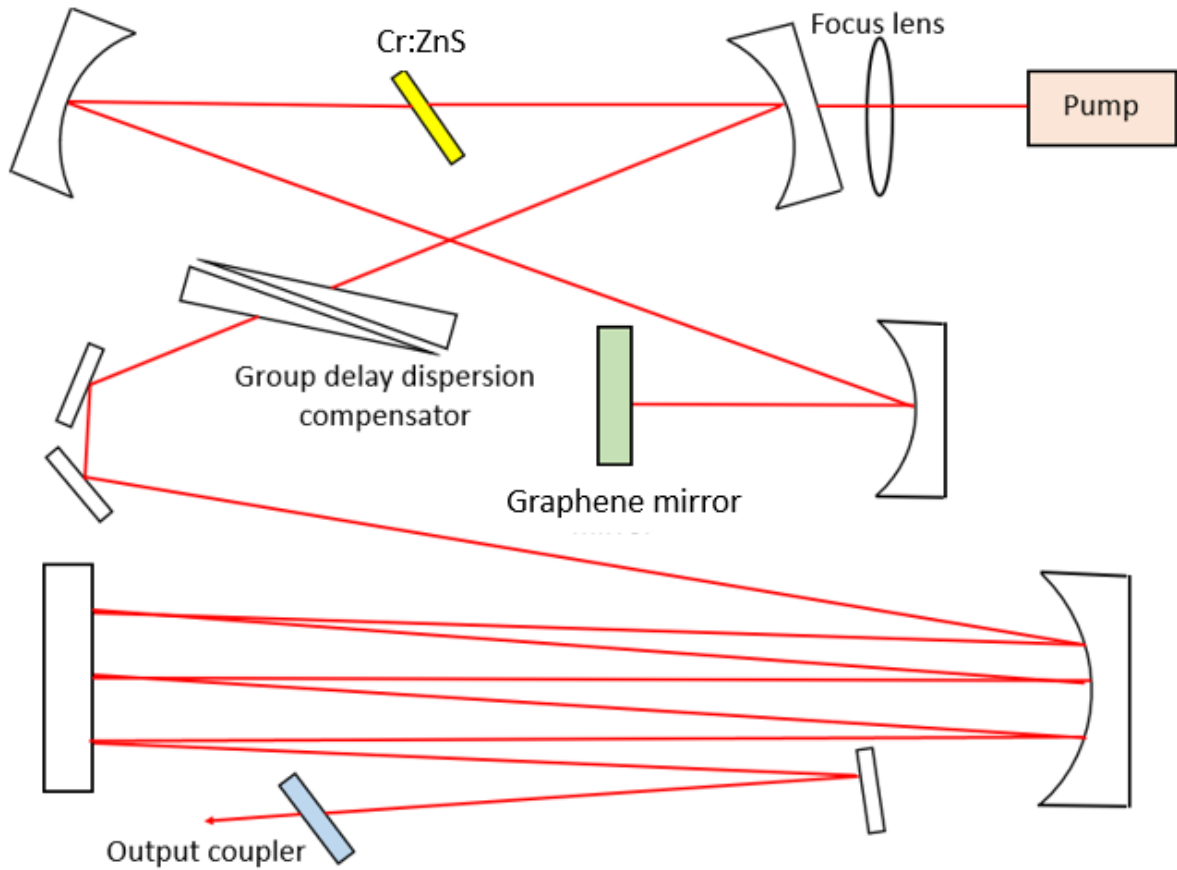


Figure 19. The extended Cr:ZnS cavity for mode-locking.

The setup of this extended cavity was built upon the standard Cr:ZnS cavity by extending the cavity length using the Herriott-type multi-pass cavity. The output coupler was replaced by another mirror to connect to the multi-pass cavity.

In the case of mode-locking using GS1, the two highly reflecting mirrors used in the multi-pass cavity had radius of curvature of 1250 mm and 5000 mm and were separated at a distance such that there were 6 passes in the multi-pass cavity. This setup using GS1 as saturable absorber was used as the laser source for the pump-probe experiment described previously.

In the case of mode-locking using GCM1, the two highly reflecting mirror were separated at a distance of 1 m with 4 bounces in the multi-pass cavity.

The performances of the graphene saturable absorber mirrors in these two mode-locking cavities are presented in the following chapter.

Chapter 5: Experimental Results and Discussion

5.1 Relaxation Times

Typically, the relaxation time of a saturable absorber has two components; a fast component denoted as τ_1 and a slow component denoted as τ_2 . In the pump-probe experiment, by varying the time delay and measuring the corresponding intensities, a graph of intensity against time delay can be plotted and fitted using a bi-exponential decay model. The values of τ_1 and τ_2 can be extracted from the bi-exponential fit.

5.1.1 SESAM and CNT

The mid-infrared picosecond laser source was used to pump and probe SESAM and CNT. At 2 μm , the published recovery times of SESAM is 63 ps for the slow component and 1.1 ps for the fast component [69]. On the other hand, CNT has approximately $\tau_1 = 0.25$ ps and $\tau_2 = 1.2$ ps [70] at the same wavelength. The τ_2 of SESAM obtained is 63 ps which is in good agreement with reported value. However, the other components of SESAM and CNT cannot be accurately resolved since those values are very close to the pulse width (1.6 ps) of the pulse laser source which sets the temporal resolution limit of the measurement. Table 1 summarises the measured and reported values of SESAM and CNT's recovery times.

Saturable absorbers	Measured values	Reported values	References
SESAM	$\tau_1 = --$ $\tau_2 = 63$ ps	$\tau_1 = 1.1$ ps $\tau_2 = 63$ ps	[69]
CNT	$\tau_1 = --$ $\tau_2 = 2.6$ ps	$\tau_1 = 0.25$ ps $\tau_2 = 1.2$ ps	[70]

Table 1. The measured and reported recovery times of SESAM and CNT.

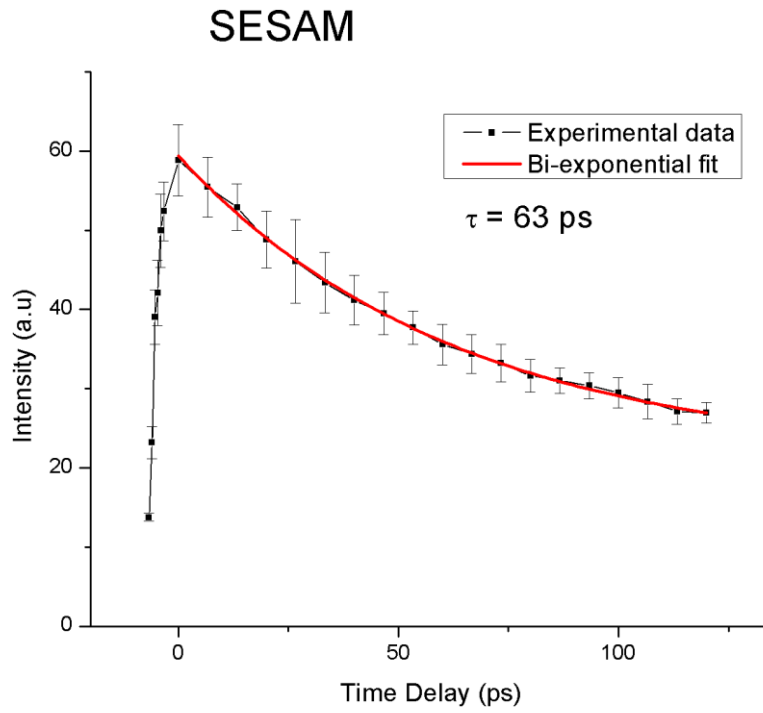


Figure 20. The relaxation dynamics of SESAM at above $2 \mu\text{m}$.

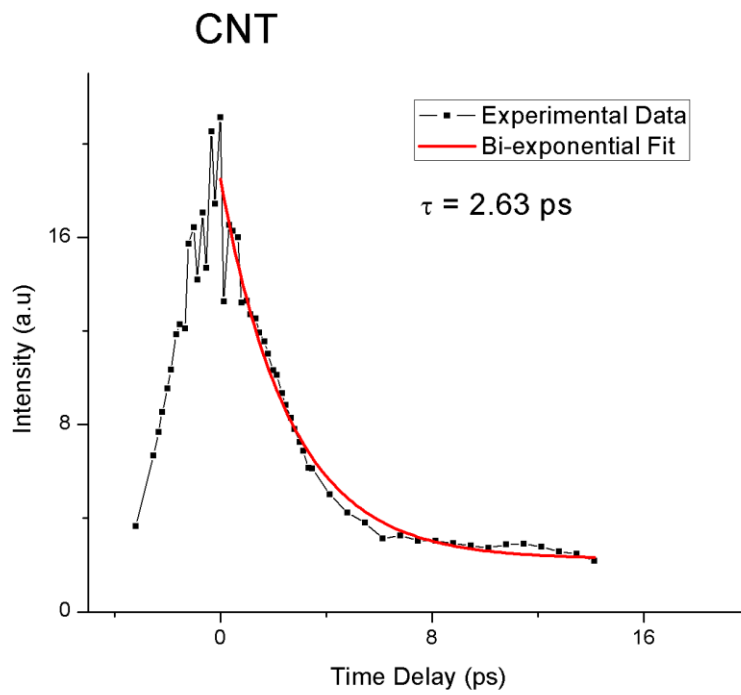


Figure 21. The relaxation dynamic of CNT at above $2 \mu\text{m}$.

5.1.2 Graphene on Sapphire Mirrors

Although graphene was transferred onto two different sapphire mirrors, one of them (GS1) was used to mode-lock the laser source for the pump-probe experiment and hence, could not be used to measure its relaxation times.

The two-layer graphene saturable absorber mirror on sapphire 2 (GS2) has a fast component of 0.15 ps and a slow component of 1.06 ps. These values are close to the average values of graphene average relaxation times ($\tau_1 = 0.168$ ps and $\tau_2 = 1.190$ ps) [69] measured at 2 μm .

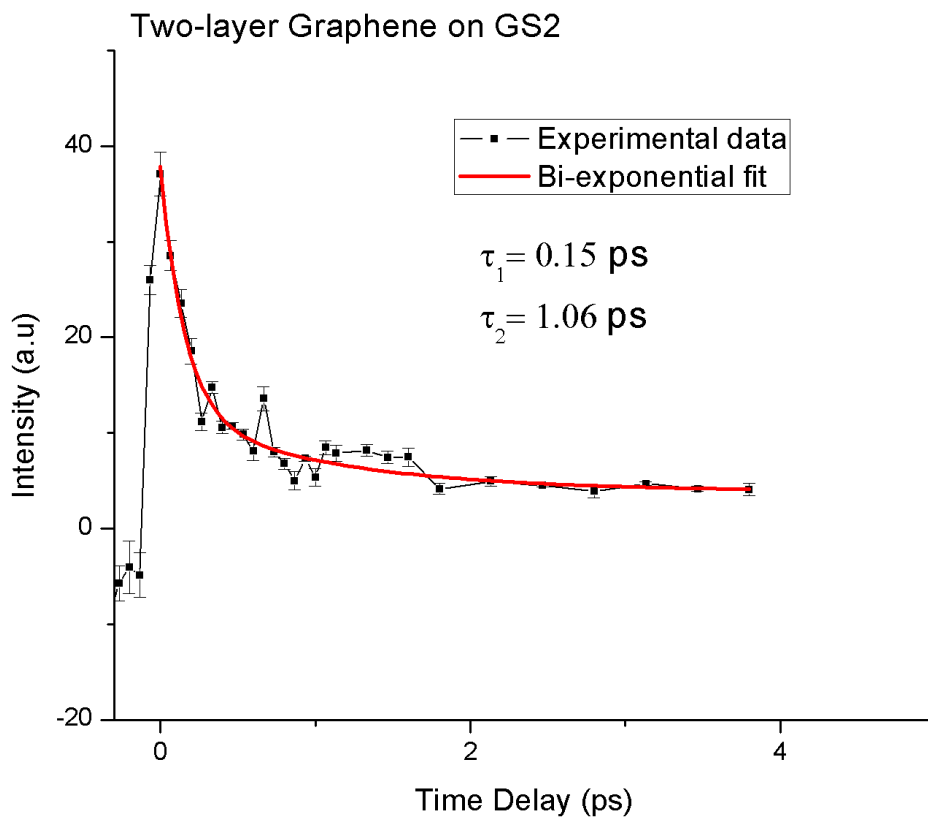


Figure 22. The relaxation dynamic of two-layer graphene on sapphire mirror 2 (GS2) at above 2 μm .

5.1.3 Graphene on Chirped Mirrors

Two layer graphene was transferred onto chirped mirror 1 (GCM1). The graphene has relaxation times of $\tau_1 = 0.21$ ps and $\tau_2 = 1.01$ ps.

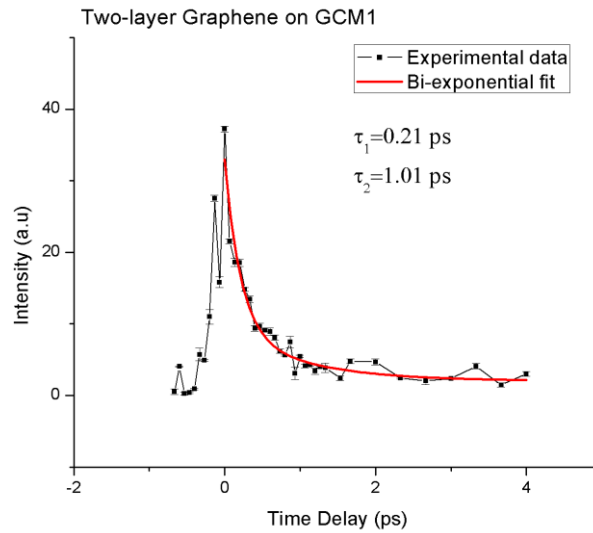


Figure 23. The relaxation dynamic of two-layer graphene on GCM1 at above $2 \mu\text{m}$.

Chirped mirror 2 (GCM2) has one section with one-layer graphene and another section with two-layer graphene. The one-layer graphene area has $\tau_1 = 0.15$ ps and $\tau_2 = 1.47$ ps and the two-layer graphene has $\tau_1 = 0.17$ ps and $\tau_2 = 1.25$ ps.

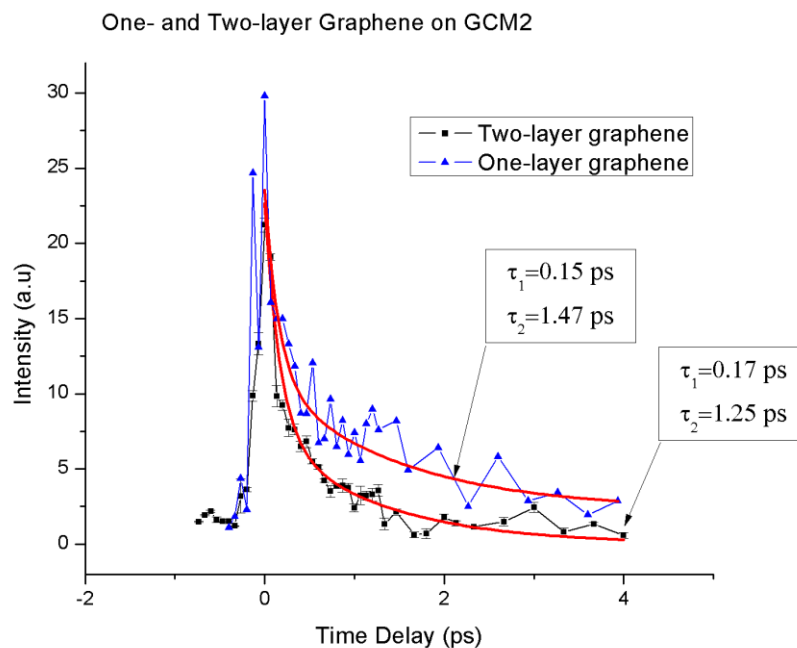


Figure 24. The relaxation dynamics of one- and two-layer graphene on chirped mirror 2 (GCM2) at above $2 \mu\text{m}$.

5.1.4 Graphene on Silver Mirror

Single-layer graphene was transferred onto the silver mirror (GAM). It exhibits a fast component of 0.16 ps and a slow component of 0.92 ps.

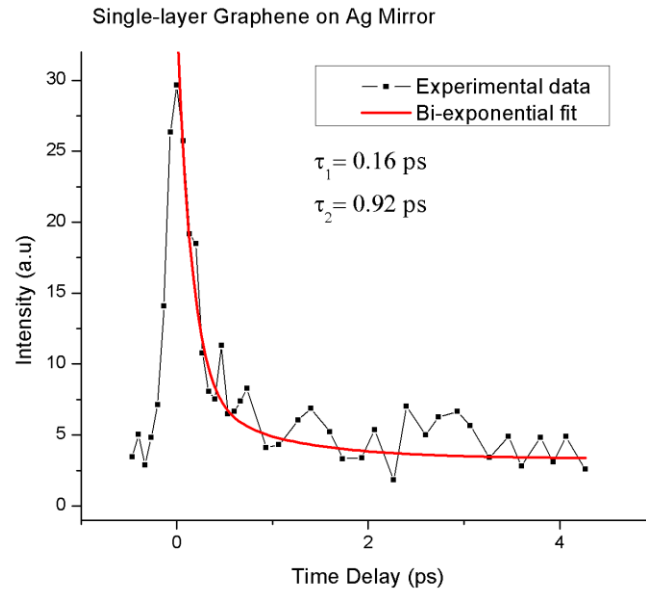


Figure 25. The relaxation dynamics of single-layer graphene on Ag mirror (GAM) at above 2 μm .

5.1.5 Summary

The recovery times of all the graphene mirrors obtained using the pump-probe technique at 2.35 μm are summarised in Table 2.

Type of mirror substrate	Number of layers of graphene	Fast component, τ_1 (ps)	Slow component, τ_2 (ps)
Sapphire 2 (GS2)	2	0.15	1.06
Chirped Mirror 1 (GCM1)	2	0.21	1.01
Chirped Mirror 2 (GCM2)	2	0.17	1.25
Chirped Mirror 2 (GCM2)	1	0.15	1.47
Silver Mirror (GAM)	1	0.16	0.92

Table 2. A summary of the fast and slow components of graphene's recovery time, measured using pump-probe technique at 2.35 μm .

The pump-probe technique employed by [69] using a 2 μm femtosecond laser reported similar recovery times of graphene. The fast component is in the range of 0.091-0.253 ps while the slow component is in the range of 0.996-1.397 ps [69].

For comparison, at 2 μm , SESAM has $\tau_1 = 1.1$ ps and $\tau_2 = 63$ ps [69] and CNT has $\tau_1 = 0.25$ ps and $\tau_2 = 1.2$ ps. In terms of pulse duration, graphene has a better ability to mode-lock ultrashort pulses. Its fast relaxation time allow graphene to recover from bleaching much quicker than other saturable absorbers.

As shown in Table 2, the presence of multilayer graphene does not affect the fast recovery times of the saturable absorber since both single and double layer graphene on GCM2 have similar recovery times for the fast component. This pattern is contradictory to the observation by [48], which showed that the relaxation time of graphene increases as the number of graphene layer increases. But in agreement with observation by [47], which reported that the slow component τ_2 of graphene's relaxation time decreases as the crystal disorder increases. The addition of another layer of graphene on GCM2 may have induced some disorder.

In addition, regardless of the mirror substrate, the fast component of the relaxation time of graphene has no considerable dependency on the type of substrates since all of the graphene mirrors have similar τ_1 values. This imply that graphene can practically be transferred onto any mirror substrate without jeopardising its relaxation time.

5.2 Mode-Locking in Cr:ZnS Laser

5.2.1 Graphene on Chirped Mirror

Using graphene on chirped mirror 1 (GCM1) as saturable absorber, the mode-locking in both the standard and extended cavity generate pulses of similar pulse duration of 110 fs (Figure 26) and similar spectral bandwidth of 50 nm (Figure 27).

In the standard cavity regime, the mode-locked laser exhibited repetition rate of 66 MHz with output power of 70 mW and pulse energy of 1.06 nJ.

In the extended cavity regime, the mode-locked laser exhibited a lower repetition rate of 14.6 MHz and lower output power of 16 mW and pulse energy of 1.1 nJ.

The fluence of the graphene chirped mirror can be estimated by using equation (10). The beam has a diameter of 120 μm and the output couple has transmission of 18%. The energy density arriving at the graphene chirped mirror saturable absorber (GCM1) is estimated to be approximately between 40-50 $\mu\text{J}/\text{cm}^2$, considering losses in the cavity and at the output coupler. Hence, the saturation fluence could be estimated even lower than 40 $\mu\text{J}/\text{cm}^2$.

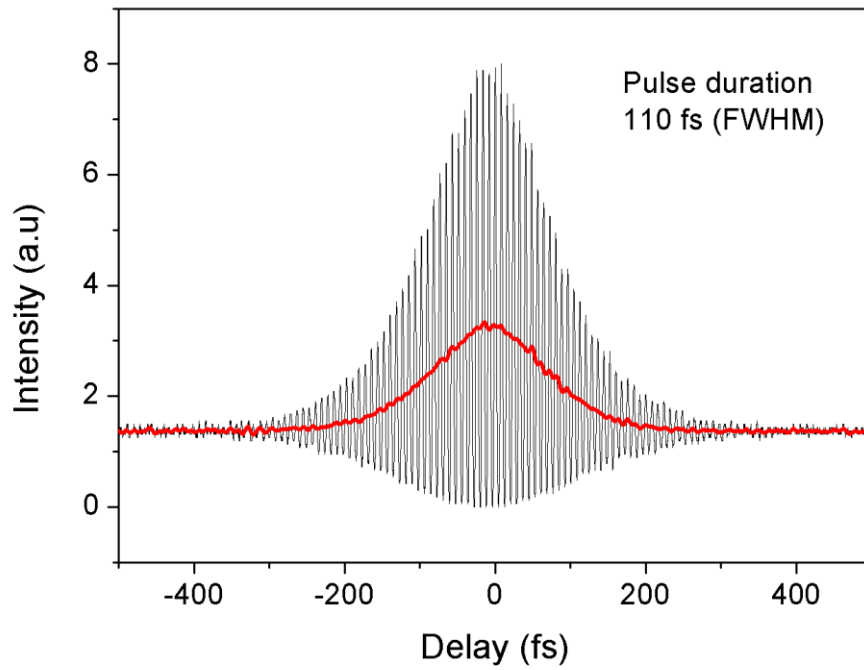


Figure 26. Autocorrelator measurement of the pulse duration using GCM1 as saturable absorber.

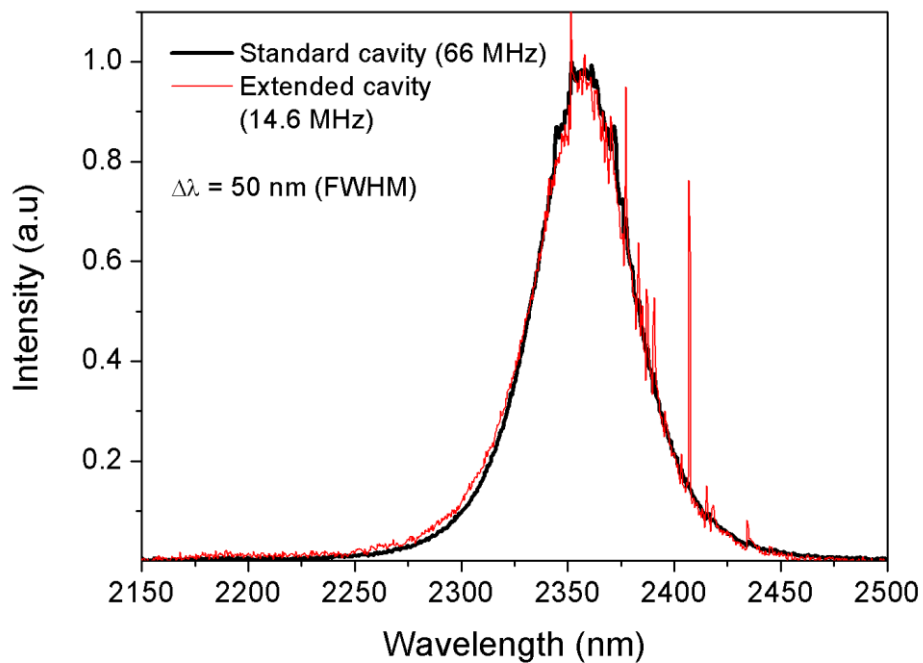


Figure 27. The optical spectra of the mode-locked laser using GCM1 as saturable absorber in the standard and extended cavities.

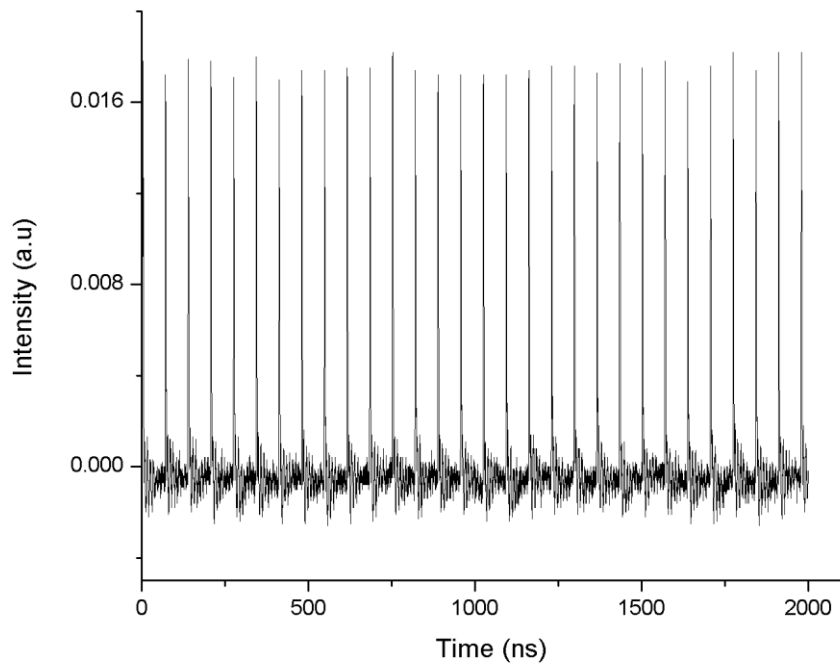


Figure 28. The pulse train in the extended cavity regime.

Chapter 6: Conclusion and Future Outlook

Graphene saturable absorber mirrors were successfully fabricated using graphene transfer method. These saturable absorbers were characterised using Raman spectroscopy. By calculating the ratio of their peaks, the level of defect can be quantified easily and also to determine the number of layers of graphene on the mirrors.

The graphene chirped mirror saturable absorber mirror was integrated into a standard cavity and an extended cavity of Cr:ZnS and mode-locking was achieved in both cases. The ability of the graphene on chirped mirror to mode-lock these lasers shows that the function of a saturable absorber and a dispersion compensator can be combined into a single optical device.

The recovery times of the graphene saturable absorber mirrors were measured using pump-probe technique. Comparison to other saturable absorbers such as SESAM and CNT showed that graphene has a faster relaxation time which is a crucial feature to generate ultrafast lasers.

There are still many more aspects of graphene saturable absorber to be explored. One of them is to properly measure the nonlinear optical parameters such as the modulation depth, saturation intensity and the non-saturable loss of these graphene mirrors to provide a more comprehensive understanding of graphene as a saturable absorber.

Another possibility is to fabricate multi-layer graphene saturable absorber mirror to investigate the influence of the number of layer of graphene on the relaxation dynamics of graphene. In order to do so, the transfer process has to be further optimized to reduce defects for higher number of layers.

For short pulse laser operating between 2-3 μm , graphene is by far the best material for saturable absorber. Its easy fabrication and transfer process, coupled with its many unique optical and electronics properties create endless possibilities for graphene-based optical devices.

References

- [1] A. Schliesser, N. Picqué, and T. W. Hänsch, "Mid-infrared frequency combs," *Nature Photonics*, vol. 6, p. 440, 06/28/online 2012.
- [2] J. Ma, G. Q. Xie, P. Lv, W. L. Gao, P. Yuan, L. J. Qian, *et al.*, "Graphene mode-locked femtosecond laser at 2 μm wavelength," *Optics Letters*, vol. 37, pp. 2085-2087, 2012/06/01 2012.
- [3] J.-L. Xu, X.-L. Li, Y.-Z. Wu, X.-P. Hao, J.-L. He, and K.-J. Yang, "Graphene saturable absorber mirror for ultra-fast-pulse solid-state laser," *Optics Letters*, vol. 36, pp. 1948-1950, 2011/05/15 2011.
- [4] G. Q. Xie, J. Ma, P. Lv, W. L. Gao, P. Yuan, L. J. Qian, *et al.*, "Graphene saturable absorber for Q-switching and mode locking at 2 μm wavelength [Invited]," *Optical Materials Express*, vol. 2, pp. 878-883, 2012/06/01 2012.
- [5] J. Ma, G. Xie, P. Lv, W. Gao, P. Yuan, L. Qian, *et al.*, "Wavelength-Versatile Graphene-Gold Film Saturable Absorber Mirror for Ultra-Broadband Mode-Locking of Bulk Lasers," *Scientific Reports*, vol. 4, p. 5016, 05/23/online 2014.
- [6] N. Tolstik, E. Sorokin, and I. T. Sorokina, "Graphene mode-locked Cr:ZnS laser with 41 fs pulse duration," *Optics Express*, vol. 22, pp. 5564-5571, 2014/03/10 2014.
- [7] W. Koechner, "Energy Transfer between Radiation and Atomic Transitions," in *Solid-State Laser Engineering*, 6th ed U.S.A: Springer, 2006.
- [8] O. Svelto, "Introductory Concepts," in *Principles of Lasers*, Fourth ed U.S.A: Plenum Press, 1998.
- [9] T. H. Maiman, "Stimulated optical radiation in ruby," 1960.
- [10] L. D. DeLoach, R. H. Page, G. D. Wilke, S. A. Payne, and W. F. Krupke, "Transition metal-doped zinc chalcogenides: spectroscopy and laser demonstration of a new class of gain media," *IEEE Journal of Quantum Electronics*, vol. 32, pp. 885-895, 1996.
- [11] I. Sorokina, "Crystalline Mid-Infrared Lasers," in *Solid-State Mid-Infrared Laser Sources*. vol. 89, ed Germany: Springer, 2003.
- [12] I. T. Sorokina, "Cr²⁺-doped II–VI materials for lasers and nonlinear optics," *Optical Materials*, vol. 26, pp. 395-412, 2004/09/01/ 2004.
- [13] I. T. Sorokina, E. Sorokin, S. Mirov, V. Fedorov, V. Badikov, V. Panyutin, *et al.*, "Continuous-wave tunable Cr²⁺:ZnS laser," *Applied Physics B*, vol. 74, pp. 607-611, April 01 2002.
- [14] W. Koechner, "Mode-Locking," in *Solid-State Laser Engineering*, 6th ed USA: Springer, 2006.
- [15] K. Sala, G. Kenney-Wallace, and G. Hall, "CW autocorrelation measurements of picosecond laser pulses," *IEEE Journal of Quantum Electronics*, vol. 16, pp. 990-996, 1980.
- [16] R. Paschotta, *Field guide to laser pulse generation* vol. 14: SPIE Press Bellingham, 2008.
- [17] L. E. Hargrove, R. L. Fork, and M. A. Pollack, "Locking of He-Ne laser modes induced by synchronous intracavity modulation," *Applied Physics Letters*, vol. 5, pp. 4-5, 1964.
- [18] T. J. Carrig, G. J. Wagner, A. Sennaroglu, J. Y. Jeong, and C. R. Pollock, "Mode-locked Cr²⁺:ZnSe laser," *Optics Letters*, vol. 25, pp. 168-170, 2000/02/01 2000.

- [19] U. Morgner, F. X. Kärtner, S. H. Cho, Y. Chen, H. A. Haus, J. G. Fujimoto, *et al.*, "Sub-two-cycle pulses from a Kerr-lens mode-locked Ti:sapphire laser," *Optics Letters*, vol. 24, pp. 411-413, 1999/03/15 1999.
- [20] D. H. Sutter, G. Steinmeyer, L. Gallmann, N. Matuschek, F. Morier-Genoud, U. Keller, *et al.*, "Semiconductor saturable-absorber mirror–assisted Kerr-lens mode-locked Ti:sapphire laser producing pulses in the two-cycle regime," *Optics Letters*, vol. 24, pp. 631-633, 1999/05/01 1999.
- [21] N. Tolstik, E. Sorokin, and I. T. Sorokina, "Kerr-lens mode-locked Cr:ZnS laser," *Optics Letters*, vol. 38, pp. 299-301, 2013/02/01 2013.
- [22] E. Sorokin, N. Tolstik, K. I. Schaffers, and I. T. Sorokina, "Femtosecond SESAM-modelocked Cr:ZnS laser," *Optics Express*, vol. 20, pp. 28947-28952, 2012/12/17 2012.
- [23] K. Kashiwagi and S. Yamashita, "Optical deposition of carbon nanotubes for fiber-based device fabrication," in *Frontiers in Guided Wave Optics and Optoelectronics*, ed: InTech, 2010.
- [24] U. Keller, "2.1 Ultrafast solid-state lasers," in *Laser Physics and Applications*, ed: Springer, 2007, pp. 33-167.
- [25] I. D. Jung, F. X. Kärtner, L. R. Brovelli, M. Kamp, and U. Keller, "Experimental verification of soliton mode locking using only a slow saturable absorber," *Optics Letters*, vol. 20, pp. 1892-1894, 1995/09/15 1995.
- [26] R. Paschotta and U. Keller, "Passive mode locking with slow saturable absorbers," *Applied Physics B*, vol. 73, pp. 653-662, November 01 2001.
- [27] H. A. Haus, J. G. Fujimoto, and E. P. Ippen, "Structures for additive pulse mode locking," *Journal of the Optical Society of America B*, vol. 8, pp. 2068-2076, 1991/10/01 1991.
- [28] U. Keller, K. J. Weingarten, F. X. Kartner, D. Kopf, B. Braun, I. D. Jung, *et al.*, "Semiconductor saturable absorber mirrors (SESAM's) for femtosecond to nanosecond pulse generation in solid-state lasers," *IEEE Journal of Selected Topics in Quantum Electronics*, vol. 2, pp. 435-453, 1996.
- [29] C. V. Shank and E. P. Ippen, "Subpicosecond kilowatt pulses from a mode-locked cw dye laser," *Applied Physics Letters*, vol. 24, pp. 373-375, 1974.
- [30] U. Keller, "Recent developments in compact ultrafast lasers," *Nature*, vol. 424, p. 831, 08/14/online 2003.
- [31] Y.-C. Chen, N. R. Ravavikar, L. S. Schadler, P. M. Ajayan, Y.-P. Zhao, T.-M. Lu, *et al.*, "Ultrafast optical switching properties of single-wall carbon nanotube polymer composites at 1.55 μm ," *Applied Physics Letters*, vol. 81, pp. 975-977, 2002.
- [32] Y. Zhenhua, W. Yonggang, Z. Xiao, D. Xinzheng, T. Jinrong, and S. Yanrong, "A 66 fs highly stable single wall carbon nanotube mode locked fiber laser," *Laser Physics*, vol. 24, p. 015105, 2014.
- [33] T. Hasan, Z. Sun, F. Wang, F. Bonaccorso, P. H. Tan, A. G. Rozhin, *et al.*, "Nanotube–polymer composites for ultrafast photonics," *Advanced Materials*, vol. 21, pp. 3874-3899, 2009.
- [34] S. Yamashita, "A Tutorial on Nonlinear Photonic Applications of Carbon Nanotube and Graphene," *Journal of Lightwave Technology*, vol. 30, pp. 427-447, 2012/02/12 2012.
- [35] G. Sobon, A. Duzynska, M. Świniarski, J. Judek, J. Sotor, and M. Zdrojek, "CNT-based saturable absorbers with scalable modulation depth for Thulium-doped fiber lasers operating at 1.9 μm ," *Scientific Reports*, vol. 7, p. 45491, 04/03/online 2017.

- [36] F. Wang, A. G. Rozhin, V. Scardaci, Z. Sun, F. Henrich, I. H. White, *et al.*, "Wideband-tuneable, nanotube mode-locked, fibre laser," *Nature Nanotechnology*, vol. 3, p. 738, 11/02/online 2008.
- [37] S. Xu, F. Wang, C. Zhu, Y. Meng, Y. Liu, W. Liu, *et al.*, "Ultrafast nonlinear photoresponse of single-wall carbon nanotubes: a broadband degenerate investigation," *Nanoscale*, vol. 8, pp. 9304-9309, 2016.
- [38] Q. Bao, H. Zhang, Y. Wang, Z. Ni, Y. Yan, Z. X. Shen, *et al.*, "Atomic-Layer Graphene as a Saturable Absorber for Ultrafast Pulsed Lasers," *Advanced Functional Materials*, vol. 19, pp. 3077-3083, 2009.
- [39] Z. Sun, T. Hasan, F. Torrisi, D. Popa, G. Privitera, F. Wang, *et al.*, "Graphene Mode-Locked Ultrafast Laser," *ACS Nano*, vol. 4, pp. 803-810, 2010/02/23 2010.
- [40] B. In Hyung, L. Hwang Woon, B. Sukang, H. Byung Hee, A. Yeong Hwan, Y. Dong-II, *et al.*, "Efficient Mode-Locking of Sub-70-fs Ti:Sapphire Laser by Graphene Saturable Absorber," *Applied Physics Express*, vol. 5, p. 032701, 2012.
- [41] G. Zhu, X. Zhu, K. Balakrishnan, R. A. Norwood, and N. Peyghambarian, "Fe²⁺:ZnSe and graphene Q-switched singly Ho³⁺-doped ZBLAN fiber lasers at 3 μm ," *Optical Materials Express*, vol. 3, pp. 1365-1377, 2013/09/01 2013.
- [42] A. Martinez and Z. Sun, "Nanotube and graphene saturable absorbers for fibre lasers," *Nature Photonics*, vol. 7, p. 842, 2013.
- [43] C. Lee, X. Wei, J. W. Kysar, and J. Hone, "Measurement of the elastic properties and intrinsic strength of monolayer graphene," *science*, vol. 321, pp. 385-388, 2008.
- [44] P. R. Wallace, "The Band Theory of Graphite," *Physical Review*, vol. 71, pp. 622-634, 05/01/ 1947.
- [45] A. H. Castro Neto, F. Guinea, N. M. R. Peres, K. S. Novoselov, and A. K. Geim, "The electronic properties of graphene," *Reviews of Modern Physics*, vol. 81, pp. 109-162, 01/14/ 2009.
- [46] R. R. Nair, P. Blake, A. N. Grigorenko, K. S. Novoselov, T. J. Booth, T. Stauber, *et al.*, "Fine Structure Constant Defines Visual Transparency of Graphene," *Science*, vol. 320, p. 1308, 2008.
- [47] J. M. Dawlaty, S. Shivaraman, M. Chandrashekar, F. Rana, and M. G. Spencer, "Measurement of ultrafast carrier dynamics in epitaxial graphene," *Applied Physics Letters*, vol. 92, p. 042116, 2008.
- [48] Q. Bao, H. Zhang, Z. Ni, Y. Wang, L. Polavarapu, Z. Shen, *et al.*, "Monolayer graphene as a saturable absorber in a mode-locked laser," *Nano Research*, vol. 4, pp. 297-307, 2011.
- [49] "Atomic-Layer Graphene as a Saturable Absorber for Ultrafast Pulsed Lasers," *Advanced Functional Materials*, vol. 19, pp. 3077-3083, 2009.
- [50] E. Malic and A. Knorr, *Graphene and Carbon Nanotubes: Ultrafast Optics and Relaxation Dynamics*: John Wiley & Sons, 2013.
- [51] K. S. Novoselov, A. K. Geim, S. V. Morozov, D. Jiang, Y. Zhang, S. V. Dubonos, *et al.*, "Electric field effect in atomically thin carbon films," *science*, vol. 306, pp. 666-669, 2004.
- [52] P. Blake, E. W. Hill, A. H. C. Neto, K. S. Novoselov, D. Jiang, R. Yang, *et al.*, "Making graphene visible," *Applied Physics Letters*, vol. 91, p. 063124, 2007.
- [53] A. C. Ferrari, J. C. Meyer, V. Scardaci, C. Casiraghi, M. Lazzeri, F. Mauri, *et al.*, "Raman Spectrum of Graphene and Graphene Layers," *Physical Review Letters*, vol. 97, p. 187401, 10/30/ 2006.

- [54] D. Graf, F. Molitor, K. Ensslin, C. Stampfer, A. Jungen, C. Hierold, *et al.*, "Spatially resolved Raman spectroscopy of single-and few-layer graphene," *Nano letters*, vol. 7, pp. 238-242, 2007.
- [55] L. M. Malard, M. A. Pimenta, G. Dresselhaus, and M. S. Dresselhaus, "Raman spectroscopy in graphene," *Physics Reports*, vol. 473, pp. 51-87, 2009/04/01/ 2009.
- [56] A. Jorio, M. Dresselhaus, R. Saito, and G. Dresselhaus, "Raman spectroscopy in graphene related systems. 2011," ed: John Wiley & Sons.
- [57] M. S. Dresselhaus, A. Jorio, M. Hofmann, G. Dresselhaus, and R. Saito, "Perspectives on carbon nanotubes and graphene Raman spectroscopy," *Nano letters*, vol. 10, pp. 751-758, 2010.
- [58] A. Reina, X. Jia, J. Ho, D. Nezich, H. Son, V. Bulovic, *et al.*, "Large area, few-layer graphene films on arbitrary substrates by chemical vapor deposition," *Nano letters*, vol. 9, pp. 30-35, 2008.
- [59] W. Regan, N. Alem, B. Alemán, B. Geng, Ç. Girit, L. Maserati, *et al.*, "A direct transfer of layer-area graphene," *Applied Physics Letters*, vol. 96, p. 113102, 2010.
- [60] M. T. Ghoneim, C. E. Smith, and M. M. Hussain, "Simplistic graphene transfer process and its impact on contact resistance," *Applied Physics Letters*, vol. 102, p. 183115, 2013.
- [61] E. Saubestre, "Copper etching in ferric chloride," *Industrial & Engineering Chemistry*, vol. 51, pp. 288-290, 1959.
- [62] Y. Lee, S. Bae, H. Jang, S. Jang, S.-E. Zhu, S. H. Sim, *et al.*, "Wafer-scale synthesis and transfer of graphene films," *Nano letters*, vol. 10, pp. 490-493, 2010.
- [63] C. Mattevi, H. Kim, and M. Chhowalla, "A review of chemical vapour deposition of graphene on copper," *Journal of Materials Chemistry*, vol. 21, pp. 3324-3334, 2011.
- [64] G.-H. Lee, R. C. Cooper, S. J. An, S. Lee, A. van der Zande, N. Petrone, *et al.*, "High-Strength Chemical-Vapor-Deposited Graphene and Grain Boundaries," *Science*, vol. 340, pp. 1073-1076, 2013.
- [65] Y.-H. Lee and J.-H. Lee, "Scalable growth of free-standing graphene wafers with copper(Cu) catalyst on SiO₂/Si substrate: Thermal conductivity of the wafers," *Applied Physics Letters*, vol. 96, p. 083101, 2010.
- [66] X. Liang, B. A. Sperling, I. Calizo, G. Cheng, C. A. Hacker, Q. Zhang, *et al.*, "Toward Clean and Crackless Transfer of Graphene," *ACS Nano*, vol. 5, pp. 9144-9153, 2011/11/22 2011.
- [67] Q. Hang, D. A. Hill, and G. H. Bernstein, "Efficient removers for poly(methylmethacrylate)," *Journal of Vacuum Science & Technology B: Microelectronics and Nanometer Structures Processing, Measurement, and Phenomena*, vol. 21, pp. 91-97, 2003.
- [68] X. Li, Y. Zhu, W. Cai, M. Borysiak, B. Han, D. Chen, *et al.*, "Transfer of large-area graphene films for high-performance transparent conductive electrodes," *Nano letters*, vol. 9, pp. 4359-4363, 2009.
- [69] G. Wang, K. Wang, B. M. Szydłowska, A. A. Baker-Murray, J. J. Wang, Y. Feng, *et al.*, "Ultrafast Nonlinear Optical Properties of a Graphene Saturable Mirror in the 2 μ m Wavelength Region," *Laser & Photonics Reviews*, vol. 11, 2017.
- [70] W. B. Cho, A. Schmidt, J. H. Yim, S. Y. Choi, S. Lee, F. Rotermund, *et al.*, "Passive mode-locking of a Tm-doped bulk laser near 2 μ m using a carbon

- nanotube saturable absorber," *Optics Express*, vol. 17, pp. 11007-11012, 2009/06/22 2009.
- [71] MicroChem. Nano PMMA and Copolymer Datasheet [Online]. Available: http://microchem.com/pdf/PMMA_Data_Sheet.pdf
- [72] G. Borin Barin, Y. Song, I. de Fátima Gimenez, A. G. Souza Filho, L. S. Barreto, and J. Kong, "Optimized graphene transfer: Influence of polymethylmethacrylate (PMMA) layer concentration and baking time on graphene final performance," *Carbon*, vol. 84, pp. 82-90, 2015/04/01/ 2015.

Appendix

A.1 Raman spectrum of CVD graphene (bottom layer)

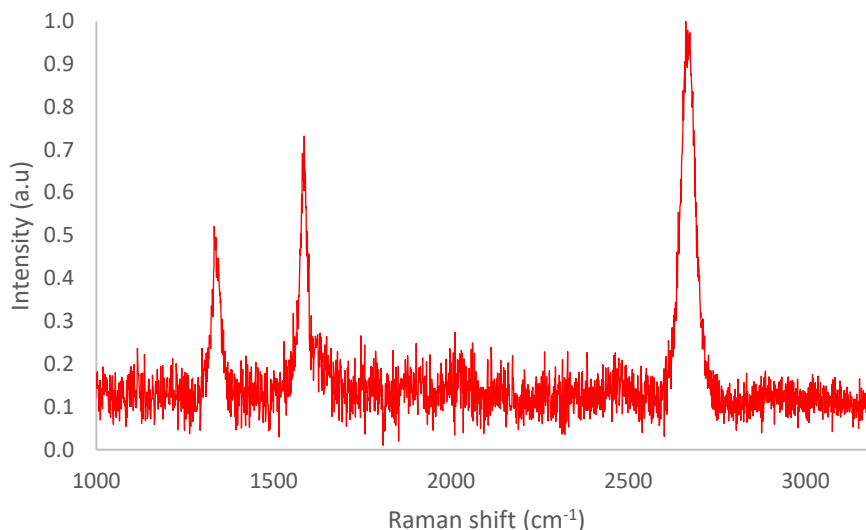
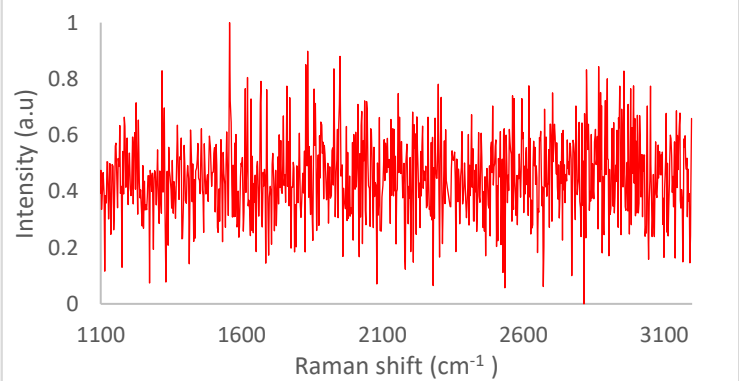
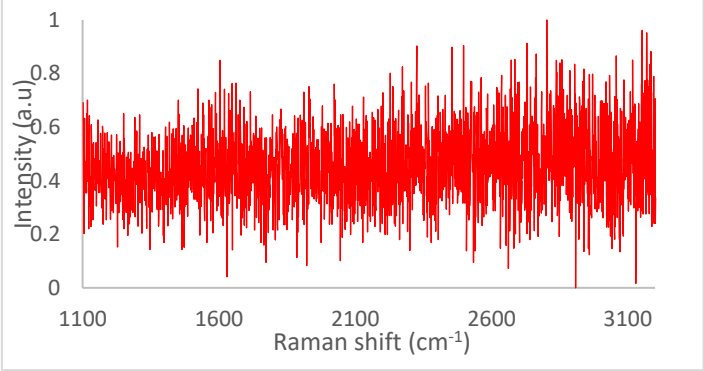
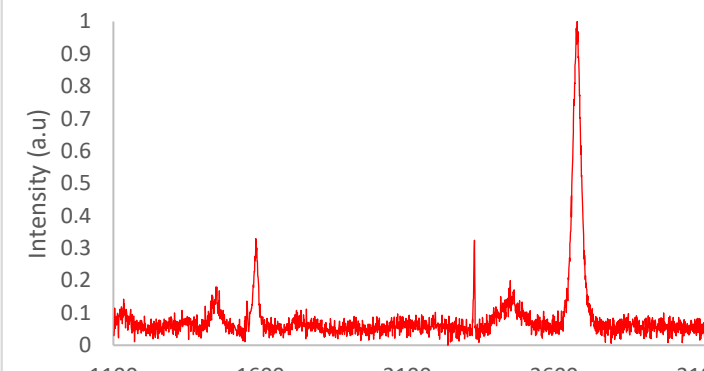
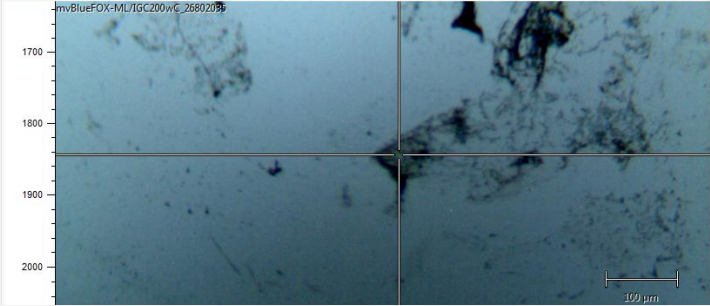
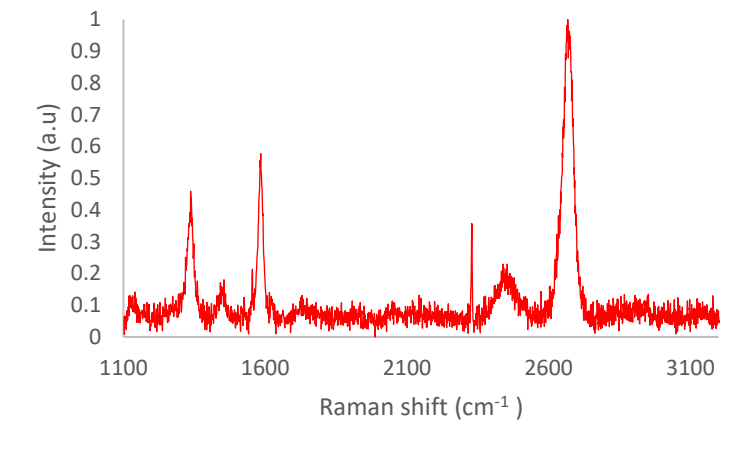
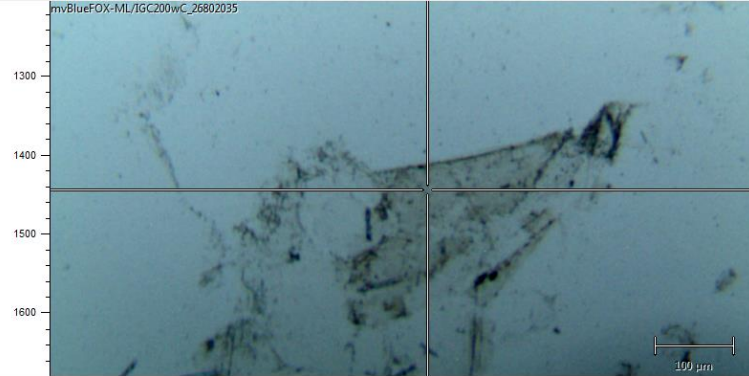
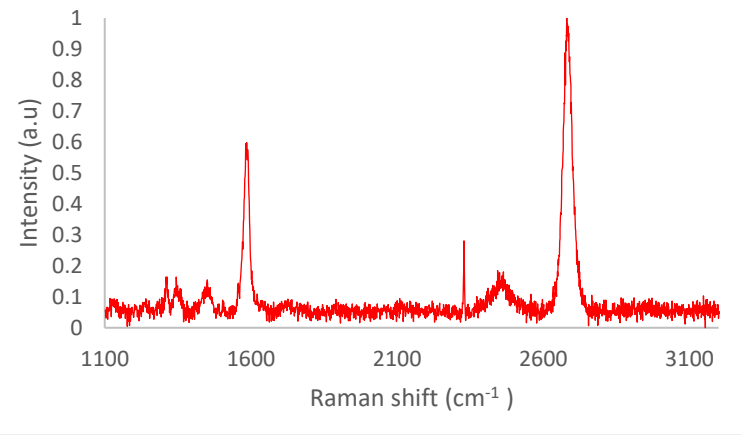


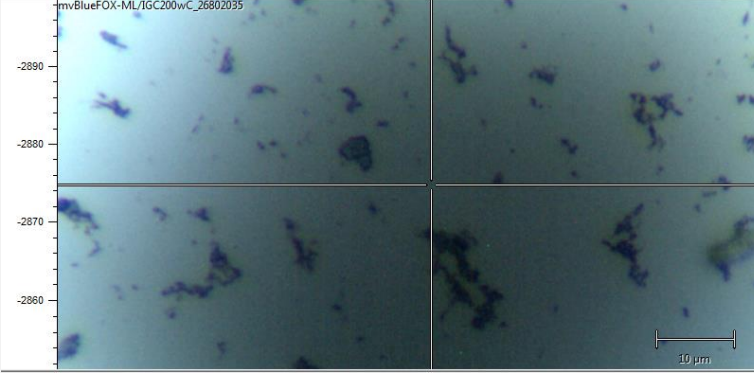
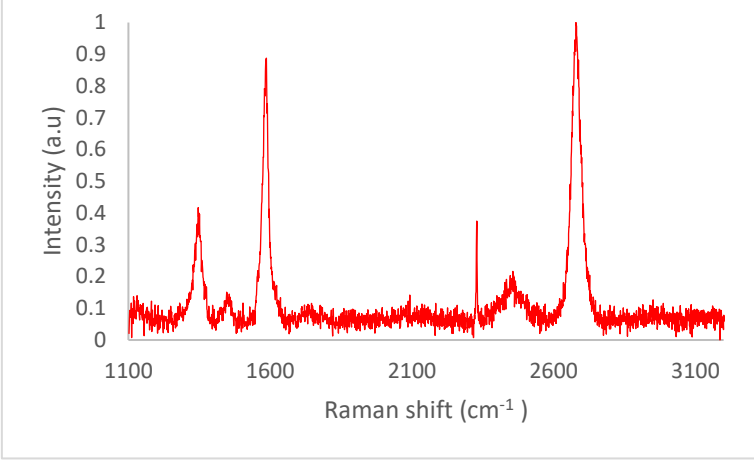
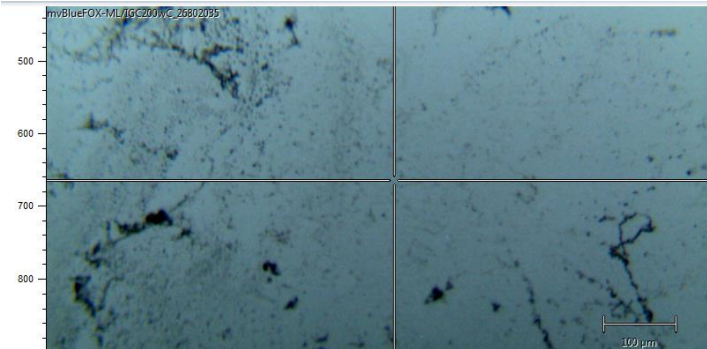
Figure 29. The Raman spectrum of as-bought graphene (back-side) with D, G and G' bands at 1336 cm^{-1} , 1580 cm^{-1} and 2670 cm^{-1} respectively. $I_D/I_G = 0.676$ and $I_G/I_{G'} = 0.715$.

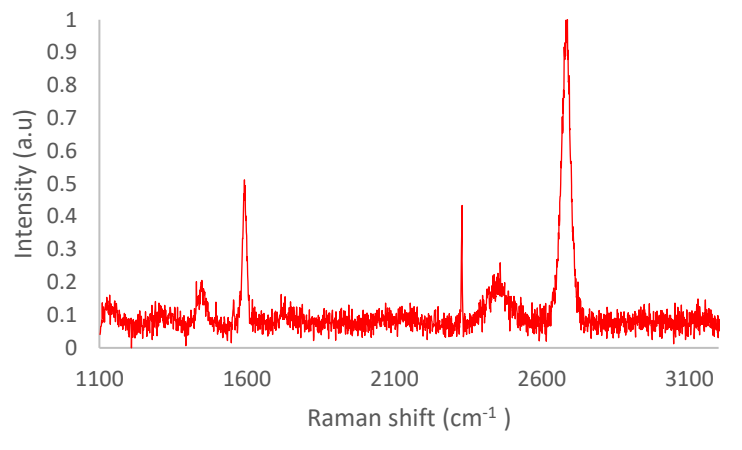
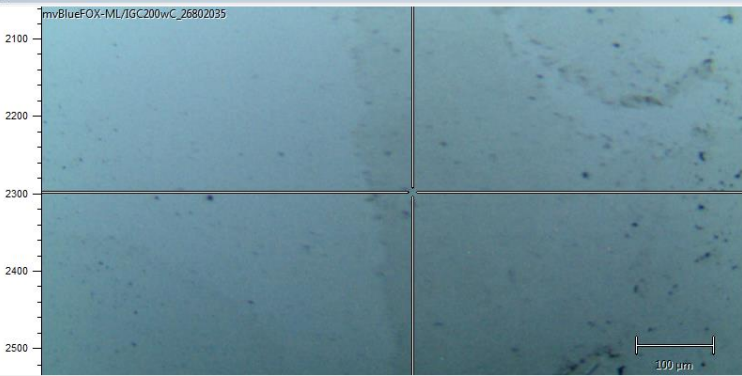
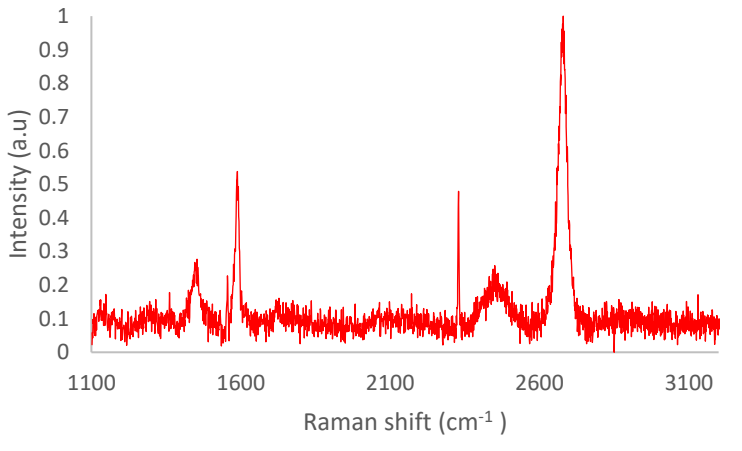
A.2 Parameters of graphene transfer using Si as substrate

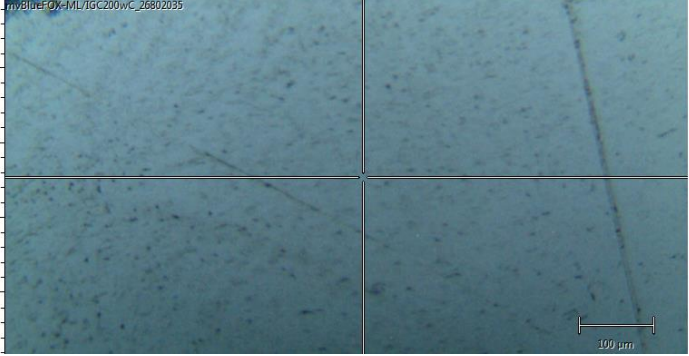
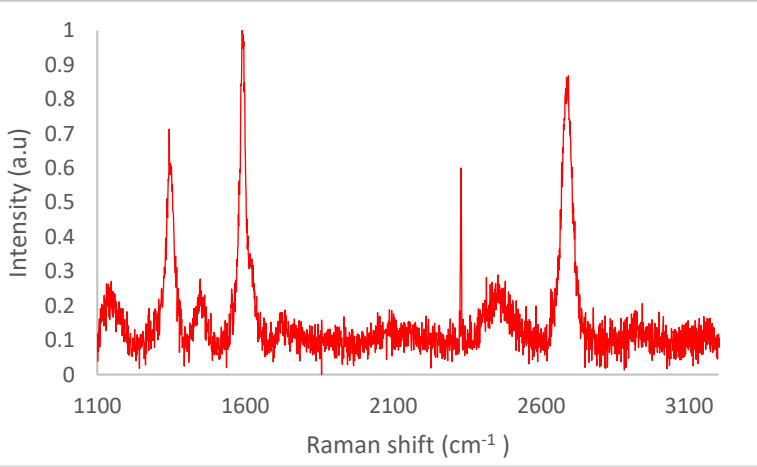
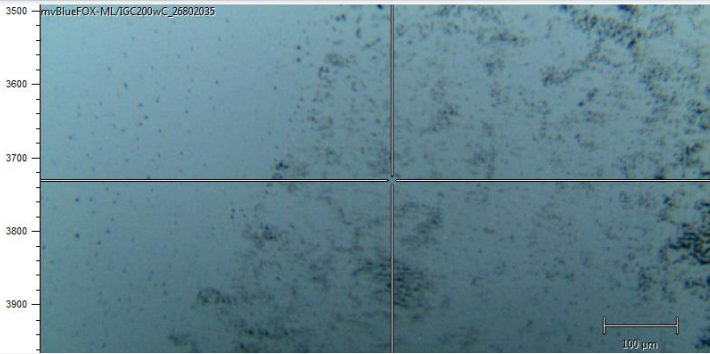
Graphene	Parameter/Condition changed	Observation and discussion
1	Type of PMMA: A12 Post-baking of PMMA: Yes Blue frame: Yes Cu Etching: overnight with magnetic stirrer at 100 rpm Plasma cleaning of substrate: No Post-transfer drying: overnight Soft-baking: 1 hour Acetone bath: 1 hour	 <p>No strong graphene peaks are observed indicating that graphene was not successfully transferred. Since this was my first attempt, I might accidentally caused major tears and cracks when handling the graphene. The graphene did not adhere fully onto the substrate and was suspected to be washed away by acetone.</p>

<p>2</p>	<p>Type of PMMA: A2 Post-baking of PMMA: No Blue frame: Yes Cu Etching: overnight with magnetic stirrer at 100 rpm Plasma cleaning of substrate: No Post-transfer drying: overnight Soft-baking: 1 hour Acetone bath: 2 hours</p>	 <p>Absence of graphene is confirmed due to no graphene peak observed from the Raman spectrum. This may be due to the use of PMMA A2 which is too thin and does not provide sufficient structural integrity. Also, the PMMA was not cured after spin-coating which further weakens the function of the polymer support.</p>
<p>3</p>	<p>Type of PMMA: A9 Post-baking of PMMA: No Blue frame: Yes Cu Etching: overnight with magnetic stirrer at 100 rpm Plasma cleaning of substrate: No Post-transfer drying: overnight Soft-baking: 1 hour Acetone bath: 2 hours</p>	 <p>Graphene G and G' bands are observed, confirming the presence of graphene. The defect band, D band (1350 cm^{-1}) was suppressed. Note that the peak on the left side of G band located at 1458 cm^{-1} is not the defect band.</p> 

		<p>Optical microscopy image at 10x optical zoom. The graphene transferred is not continuous and has folds. Some PMMA residue can also be seen.</p>
<p>4</p>	<p>Type of PMMA: A12 Post-baking of PMMA: No Blue frame: Yes Cu Etching: overnight with magnetic stirrer at 100 rpm Plasma cleaning of substrate: No Post-transfer drying: overnight Soft-baking: 1 hour Acetone bath: 2 hours</p>	 <p>Graphene D, G and G' peaks are sharp. The level of defect, $I_D/I_G = 0.670$ is high. $I_G/I_{G'} = 0.586$.</p>  <p>Less residue of PMMA than Graphene 4. Graphene is folded.</p>
<p>5</p>	<p>Type of PMMA: A2 Post-baking of PMMA: Yes Blue frame: Yes Cu Etching: overnight with magnetic stirrer at 100 rpm Plasma cleaning of substrate: No Post-transfer drying: overnight Soft-baking: 1 hour Acetone bath: 2 hours</p>	 <p>G and G' bands are very sharp. The D peak can be seen but relatively weak. The level of defect, $I_D/I_G = 0.211$. $I_G/I_{G'} = 0.605$.</p>

		
		<p>At 100x optical zoom, some PMMA residue can still be seen. At lower optical zoom, the graphene coverage is not continuous and appear only at certain regions.</p>
<p>6</p>	<p>Type of PMMA: A9 Post-baking of PMMA: Yes Blue frame: Yes Cu Etching: overnight with magnetic stirrer at 100 rpm Plasma cleaning of substrate: No Post-transfer drying: overnight Soft-baking: 1 hour Acetone bath: 2 hours</p>	 <p>Graphene peaks are present with the level of defect, $I_D/I_G = 0.442$. $I_G/I_{G'} = 0.875$.</p>  <p>It has more graphene coverage than Graphene 1,2,3,4 and 5, although some PMMA residue and cracks can still be seen.</p>

<p>7</p>	<p>Type of PMMA: A12 Post-baking of PMMA: Yes Blue frame: Yes Cu Etching: overnight with magnetic stirrer at 100 rpm Plasma cleaning of substrate: No Post-transfer drying: overnight Soft-baking: 1 hour Acetone bath: 2 hours</p>	 <p>G and G' bands are very sharp, but D band is not obvious. $I_G/I_{G'} = 0.479$.</p>  <p>The coverage of graphene appears continuous and have less residue of PMMA. Tear can still be seen. It could be due to vigorous etching condition. Etching time will be reduced at the next attempt.</p>
<p>8</p>	<p>Type of PMMA: A12 Post-baking of PMMA: Yes Blue frame: Yes Cu Etching: 2 hours with magnetic stirrer at 50 rpm Plasma cleaning of substrate: Yes Post-transfer drying: overnight Soft-baking: 2 hours Acetone bath: 4 hours</p>	 <p>D band is not clearly visible. G and G' bands are very sharp. $I_G/I_{G'} = 0.516$.</p>

		 <p>Very good coverage of graphene and very little PMMA residue. This could be due to longer soaking in acetone bath to remove the PMMA. Cracks and tears are reduced as well due to gentler etching.</p>
<p>9</p>	<p>Type of PMMA: A9 Post-baking of PMMA: Yes Blue frame: Yes Cu Etching: 2 hours with magnetic stirrer at 50 rpm Plasma cleaning of substrate: No Post-transfer drying: overnight Soft-baking: No Acetone bath: 4 hours</p>	 <p>D, G and G' bands are clearly visible. The level of defect, $I_D/I_G = 0.753$ is high. $I_G/I_{G'} = 1.12$.</p>  <p>Distribution of the graphene is very uneven.</p>

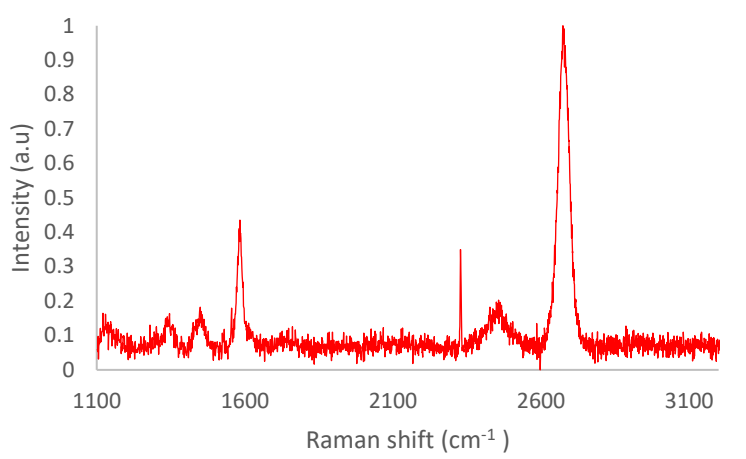
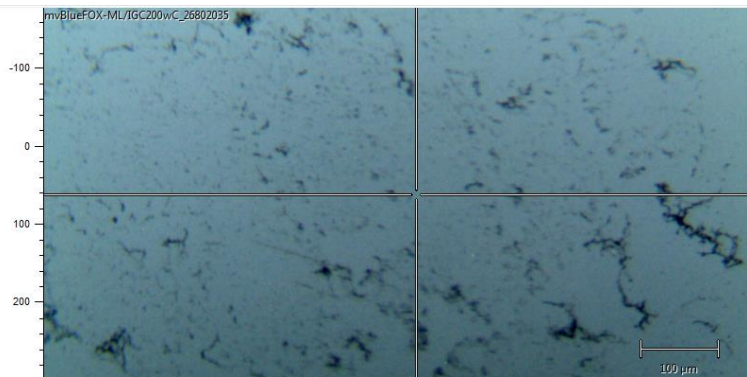
<p>10</p>	<p>Type of PMMA: A9 Post-baking of PMMA: Yes Blue frame: Yes Cu Etching: 2 hours with magnetic stirrer at 50 rpm Plasma cleaning of substrate: No Post-transfer drying: overnight Soft-baking: Yes Acetone bath: 4 hours</p>	 <p>D band is present although relatively weak. G and G' are very sharp. The level of defect, $I_D/I_G = 0.322$. $I_G/I_{G'} = 0.410$.</p>  <p>Better distribution of graphene compared to Graphene 9 due to soft-baking. However, there are still some small areas not covered and PMMA residues are very obvious.</p>
------------------	--	--

Table 3. The summary of attempts to transfer graphene onto Si wafer, by changing different kind of parameters.

From all the 10 attempts, the use of PMMA A12 as the support layer produced the best transfer. The transferred graphene using PMMA A12 does not have the defect band (D band) on its Raman spectrum and the optical microscopy image shows good graphene coverage and very little PMMA residue. Spin-coating at a speed of 6000 rpm, yield thickness of approximately 100 nm, 1500 nm and 500 nm using PMMA A2, A9 and A12 respectively [71]. PMMA A12 has the right thickness; being not too thin that it breaks easily and not too thick that it is difficult to be removed at the end. Also, PMMA A9 has higher tendency to leave more residue post-removal.

However, regardless of the choice of PMMA, post-baking after spin-coating of PMMA produced cleaner transfer (Table 3). Post-baking evaporates any residual solvent of the PMMA on the graphene which may contaminate the transfer.

During the first few initial attempts of graphene transfer, the copper was left to be etched overnight using magnetic stirrer at 100 rpm. This etching setup was too vigorous as the transferred graphene suffered lots of tear and cracks. Subsequent attempts were conducted using gentler approach. The PMMA/graphene/copper film was left in the etchant for 2 hours and the magnetic stirring was reduced to 50 rpm. As a result, this approach produced transfers with significantly less tear and better graphene coverage.

The influence of soft-baking after transferring graphene onto substrate was tested as well. Using the same PMMA, soft-baking post-transfer yield graphene with better substrate coverage and less defect as indicated by its smaller D band on the Raman spectrum. The purpose of soft-baking is to remove water that is hindering full contact between graphene and the substrate. Unattached regions will break apart when the PMMA layer is removed, creating uneven coverage of graphene, as seen on the optical microscopy image of the graphene transfer without soft-baking. The importance of this soft-baking step is frequently highlighted and investigated [66] [72].

The contact between graphene and substrate was further improved by increasing the hydrophilicity of the substrate via oxygen plasma cleaning, which helps to distribute the water evenly during the transfer process.

During the removal of PMMA in acetone bath, longer period of acetone immersion reduced PMMA residues. Optical microscopy images of graphene immersed in acetone for 4 hours show less PMMA residues than the ones immersed in acetone for 2 hours.

Overall, it can be concluded that the best parameter to transfer graphene onto a Si wafer substrate is to spin-coat PMMA A12 (~ 500 nm) as a supportive layer, followed by baking on hotplate for 10 minutes at temperature of 105 °C. Additional support using a frame of blue tape enhanced the structural support making the transfer safer. Long etching time and vigorous stirring degrades the graphene. 2 hours of etching accompanied by 50 rpm stirring is sufficient to etch the copper substrate away. Cleaning the target substrate by oxygen plasma cleaner is recommended before transferring the graphene onto the substrate. After the transfer, the sample is left to dry overnight and then soft-baked to remove trapped water. Finally, the PMMA support layer is removed in an acetone bath for 4 hours.